

BRIGHT

Erasmus+ strategic partnership for Higher Education

**BOOSTING THE SCIENTIFIC EXCELLENCE AND INNOVATION
CAPACITY OF 3D PRINTING METHODS IN PANDEMIC PERIOD**

MODULE 2 CAE

Project Title	Boosting the scientific excellence and innovation capacity of 3D printing methods in pandemic period 2020-1-RO01-KA226-HE-095517
Output	IO1 - BRIGHT e-learning support courses for curriculum aiming to boost the scientific excellence and innovation of 3D printing methods used for developing and producing medical parts in pandemic period
Module	Module 2 CAE
Date of Delivery	July 2021
Authors	Associate prof.dr.eng. Răzvan Păcurar, Associate prof.dr.eng. Nikola Korunovic, Lecturer dr.eng. Cristina Borzan, Lecturer dr.eng. Horea Chezán, Lecturer dr.eng. Vilău Cristian
Version	Final version, 17.07.2021

Content

1.	Introduction. Use and role of the Finite Element Method for medical applications based on 3D printing (AM) technologies	4
2.	Solidworks Simulation used to validate the design of a hand orthosis made by Fused Deposition Modeling technology	6
3.	Finite element analyses for medical applications using ANSYS	10
3.1.	General presentation of the ANSYS FEA program	10
3.2.	Finite Element Analysis of pelvic implants made by 3D printing	10
3.3.	Design study of anatomically shaped lattice scaffolds for the bone tissue recovery ..	22
3.3.1.	Introduction	22
3.3.2.	Lattice scaffold design concept	23
3.3.3.	CAD models	24
3.3.4.	Sensitivity study of fully wrapped ASLS design elastic properties to principal parameters changes	26
3.3.5.	Sensitivity study of realistic shape lattice scaffold elastic properties to change of struts angle	30
3.3.6.	Production using additive manufacturing technologies	33
3.3.7.	Conclusions	34
3.4.	Mechanical behavior of a dynamically stressed customized skull implant made from different types of biomaterials by SLS and vacuum casting methods	34
3.4.1.	Choosing the type of interaction between models	42
3.4.2.	Determination of the experiment period	46
3.4.3.	Results	48
3.5.	Finite element analysis to determine the mechanical characteristics of cervical discs	54
4.	Finite element analyses for medical applications using ABAQUS	64
4.1.	Structural analysis of a bone fixator	64
4.1.1.	General introduction about basics and use of ABAQUS FEA program for medical applications	64
4.1.2.	Use of ABAQUS in structural analysis of a bone fixator	64

This project has been funded with support from the European Commission. This publication [communication] reflects the views only of the authors, and the Commission cannot be held responsible for any use which may be made of the information contained therein.

4.1.3.	Creating the CAD model of femur based on CT images	66
4.1.3.1.	Creating the polygonal model of the femur	66
4.1.3.2.	Creating the CAD model of the femur	68
4.1.4.	Meshing and defining of the material characteristics	69
4.1.4.1.	Defining material characteristics	69
4.1.4.2.	Approach 1 to assigning material characteristics to femur – used for comparison with approach 2	71
4.1.4.3.	Approach 2 to assigning material characteristics to femur – used in current research	72
4.1.5.	Creating FE model of femur-fixator assembly	73
4.1.6.	Loads and boundary conditions	75
4.1.7.	Analysis results	76
4.1.8.	Conclusions	76
4.2.	Finite element analysis to estimate the behaviour of lattice structures used for manufacturing hip implants by SLM 3D printing method	77
References	85

This project has been funded with support from the European Commission. This publication [communication] reflects the views only of the authors, and the Commission cannot be held responsible for any use which may be made of the information contained therein.

1. Introduction. Use and role of the Finite Element Method for medical applications based on 3D printing (AM) technologies

The Finite Element Method (FEM) is a numerical procedure used for solving engineering and mathematical problems. FEM is usually applied in structural analysis, heat transfer, fluid flow, mass transport or electromagnetic potential problems. This procedure uses numerical strategies for solving partial differential equations in one, two or three-dimensional spaces. FEM converts a continuous problem into a set of algebraic equations defined over a division of the analysis domain called finite element mesh. In general, the solution of the discrete problem is more accurate when the number of the finite elements is higher [BIZ18].

Discretization is a method applied in mathematics and consists in transferring continuous functions, models, variables or equations into discrete counterparts. In other words, discretization represents a partitioning of the analysis domain into smaller regions called finite elements. The finite elements form together a mesh which behaves as a support for solving real engineering problems. In practical applications, the discretization frequently involves generating thousands or even more finite elements. Under such circumstances, this process is performed by finite element programs running on digital computers. When applied for solving a problem, FEM is usually called Finite Element Analysis (FEA). FEA has a substantial impact in the field of mechanical engineering, by reducing the time spent to take a product from the concept stage to the production line [BIZ18].

In mechanical engineering, FEA is used for evaluating the strain and stress states occurring in solid structures subjected to static or dynamic loads. This procedure is used by engineers to reduce the number of physical prototypes and optimize components to obtain and develop better products in a short time. FEA provides approximate solutions for problems and gives numerical values to determine the behavior of a part under given conditions. It is used in modern simulation to discover weak spots, overstressed areas, or other problems, in different domains, such as automotive, aeronautical or biomechanical industries. Currently, there are many computer programs used for finite element analysis including: ANSYS, NASTRAN, ALGOR, ABAQUS, SolidWorks Simulation etc.

If an FEM program integrated in a CAD system is used to perform a finite element analysis, the following steps must be taken:

- Building the 3D model of the physical body that is subjected to the analysis (the model can be elaborated using the facilities provided by the CAD program)

This project has been funded with support from the European Commission. This publication [communication] reflects the views only of the authors, and the Commission cannot be held responsible for any use which may be made of the information contained therein.

- Choosing the constitutive models for the materials involved in the problem to be solved and specifying the necessary physical constants (for example, elasticity problems usually involve Hooke's constitutive model described by two material constants: Young's modulus and Poisson's ratio)
- Specifying the external loads to which the body is subjected (in the case of elasticity problems, external loads are forces, pressures or torques)
- Specifying the kinematic constraints of the body (in the case of elasticity problems, these constraints refer to supports that restrain the motion)
- Discretization of the spatial domain occupied by the body using finite elements (this operation is automated by the FEM program)
- Solving the set of algebraic equations which approximates the behavior of the discretized body
- Interpretation of the numerical results obtained by the FEM program (modern computer programs provide various types of colored diagrams to assist the user in the interpretation of the numerical results; in the case of elasticity problems, these diagrams provide information about the spatial distribution of particle displacements, or stress and strain components).

This project has been funded with support from the European Commission. This publication [communication] reflects the views only of the authors, and the Commission cannot be held responsible for any use which may be made of the information contained therein.

2. Solidworks Simulation used to validate the design of a hand orthosis made by Fused Deposition Modeling technology

The fused deposition modeling (FDM) technology has been adopted for the realization of the hand orthosis. The following steps must be performed to produce a customized orthosis (see also Figure 2.1):

1. Radiographic investigation of the arm to localize the fracture and establish the diagnostic and treatment (this task is performed by an orthopedic doctor)
2. Optical scanning of the arm
3. Designing the orthosis using a CAD program
4. Choosing the system to be used for fixing the components
5. Performing a finite element analysis to determine the distribution of the von Mises equivalent stress in the orthosis
6. Importing the scanned model of the arm in “*.STL” format within the Ultimaker Cura 3.6 program
7. Establishing the technological parameters of the AM process
8. Choosing the material to be used for manufacturing the orthosis
9. Producing the orthosis by FDM
10. Manual cleaning of the orthosis (removing the supports).

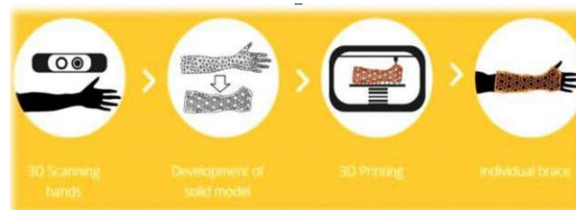


Fig. 2.1. Stages involved in the production of a personalized orthosis by AM [WWW01]

Radiographic investigations are needed for establishing the gravity of the fracture, for localizing the fracture and the placement of joints. In the case under analysis, as shown in Figure 2.2, a closed fracture was identified (marked with an arrow in Figure 2.2). Such a fracture does not require a surgical intervention. The orthosis is used in the convalescence period, being required after using the gypsum apparatus.

The 3D scanning of the arm has been performed with the Go!SCAN 3D 50TM device available at the Faculty of Machine Building at the Technical University of Cluj-Napoca (TUCN). The Vxelements program has been used for post-processing the scanning data. A complex model of the arm surface has been obtained (Fig. 2.3). The accuracy of the triangulated representation obtained in this manner is 30 μm . The arm has been kept in the same position during the scanning process. Different types of objects have been used for delimiting the scanned area (see the right picture shown in Figure 2.3).



Fig. 2.2. Radiographic investigation of the fractured arm

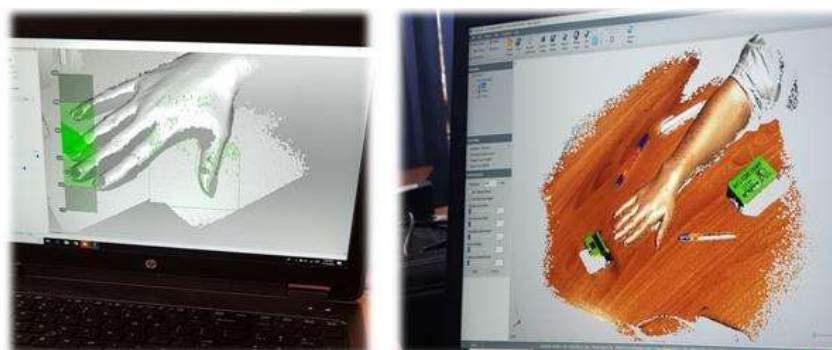


Fig. 2.3. 3D scanning of the fractured arm and delimitation of the scanning area

The scanned model has been smoothed using the Meshmixer program (Fig. 2.4). The negative model has been then generated with SolidWorks (Fig. 2.5). As one may notice in Fig. 5, the CAD model has been also adjusted to become more aesthetic. In the end, the model of the orthosis has been exported as an “*.STL” file to be used for the AM process.

The hole pattern that covers the orthosis ensures the ventilation of the arm. The size of the holes and the distance between them (in the range 4-10 mm) has been established such that the mechanical strength of the orthosis remains unaffected (and considering the technological constraints enforced by the 3D printing equipment).

This project has been funded with support from the European Commission. This publication [communication] reflects the views only of the authors, and the Commission cannot be held responsible for any use which may be made of the information contained therein.

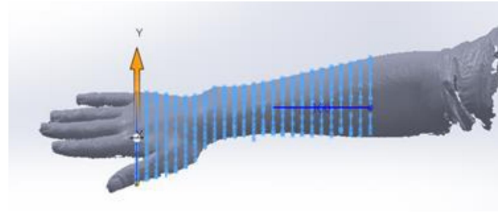


Fig. 2.4. Scanned surfaces smoothed by the Meshmixer program

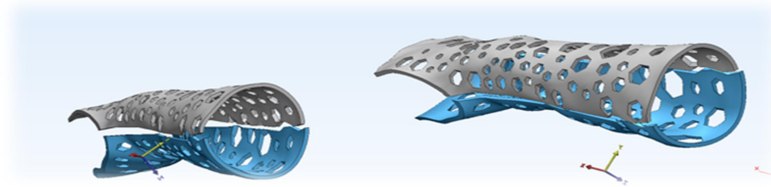


Fig. 2.5. 3D model of the orthosis generated with SolidWorks

The finite element program SolidWorks Simulation has been used to assess the mechanical strength of the orthosis. A static analysis has been performed assuming that the device is made from PLA. The physical parameters of this material have been taken from the website of the producer (Fig. 2.6).

Property	Value	Units
Shear Modulus	318.9	N/mm ²
Mass Density	1300	kg/m ³
Tensile Strength	37	N/mm ²
Compressive Strength		N/mm ²
Yield Strength	35.9	N/mm ²
Thermal Expansion Coefficient	4.1e-005	/K
Thermal Conductivity	0.13	W/(m·K)
Specific Heat	1386	J/(kg·K)

Fig. 2.6. Physical parameters of PLA material used in the finite element analysis
[WWW02]

The kinematical constraints and external loads have been imposed as shown in Fig. 2.7. One may notice that a total force of 20 N has been assumed to act on the orthosis.

The distribution of the von Mises equivalent stress resulted from the finite element analysis is shown in Fig. 2.8. One may notice that the maximum value of the stress (10.02 MPa) is considerably lower than the yield strength of PLA (35.9 MPa – see Figure 2.6).

The STL representation of the orthosis has been imported in the Ultimaker Cura 3.6 program. This program has been subsequently used to orient the model and prepare it for

manufacturing on the fused deposition modeling (FDM) equipment available at the Department of Manufacturing Engineering from the Technical University of Cluj-Napoca (Fig. 2.9).

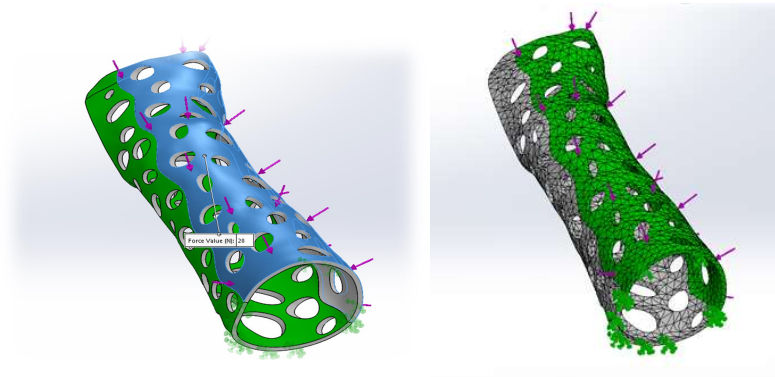


Fig. 2.7. Kinematical constraints and external loads applied to the finite element model of the orthosis

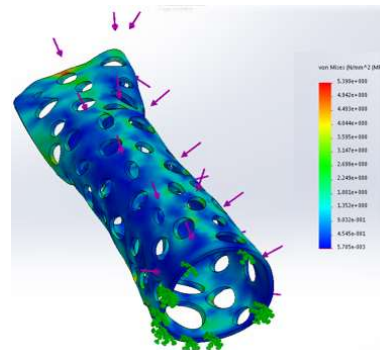


Fig. 2.8. Distribution of the von Mises equivalent stresses resulted from the finite element analysis of the orthosis



Fig. 2.9. Customized arm orthosis produced by FDM

This project has been funded with support from the European Commission. This publication [communication] reflects the views only of the authors, and the Commission cannot be held responsible for any use which may be made of the information contained therein.

3. Finite element analyses for medical applications using ANSYS

3.1. General presentation of the ANSYS FEA program

One of the most important simulation software is ANSYS. ANSYS is a global company which develops and sells engineering simulation software for design, test and operates products from different industries. ANSYS is a software package used for numerical simulation in product development. This software realizes all steps of Computer Aided Engineering (CAE) simulation along to Fluid Dynamic Simulation technology, Structural Mechanics, Electromagnetics, System Simulation or Temperature. The software is integrated and used in many industries as mechanical industry, aerospace, automotive, energy or ship building. ANSYS Mechanical Finite Element Analysis is used for computer models or structures simulations and for analyzing strength, elasticity, toughness, temperature distribution or other mechanical characteristics. Following the results obtained by simulation the functionality of a product can be established. ANSYS was used for the testing simulation of samples that were designed as presented in what follows [THO17].

3.2. Finite Element Analysis of pelvic implants made by 3D printing

A significant research that was realized by the Orthopaedic Oncology Clinic, Specific Organs Center Branch, National Cancer Center, in Korea, investigated by Finite Element Analysis (FEA) the biomechanics of a plate introduced in a 3D printed pelvic implant.

A 53-year-old woman was diagnosed with “high grade spindle cell sarcoma on left pelvic bone and proximal femur”, the solution being a “3D-printed titanium acetabular implant” [PAR19]. For realizing the simulation of the pelvic implant, the researchers have reconstructed the pelvis model using Computerized Tomography (CT) scans. Fig. 3.1 shows the radiography and CT scans of sarcoma resection area, the affected area being surrounded by a red circle.



Fig. 3.1 – (a) Plain radiography, (b) CT scan images [PAR19]

The 3D model of periacetabular implant was designed using the MIMICS software. Fig. 3.2 presents the pelvic bone in grey color and the implant in yellow color. For fixing the implant in the hip bone, straight-type plates and horseshoe-shaped plates were designed (also shown in Fig. 3.2).

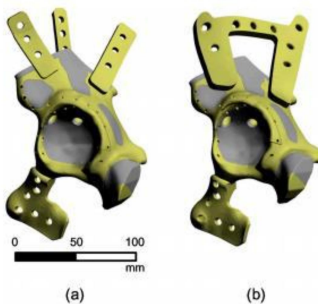


Fig. 3.2. 3D model of the periacetabular implant and the fixation of the plates: (a) the straight-type plates, (b) the horseshoe-shaped plates [PAR19]

The finite element analysis was performed using ANSYS. Fig. 3.3 shows the boundary conditions imposed onto the finite element model: the cortical bone is presented with yellow color, cancellous bone with blue color, straight-type plate model with purple color and finally horseshoe-shaped plates with orange color. The hemi-pelvis was fixed by the pubis and femoral head, indicated with green color in Fig. 3.3. The contact between pelvis and implant was considered as “bonded” and the contact between the femoral head and acetabulum was considered as “frictionless”. A distributed load of 4.9 KN was applied on the head of the iliac bone. This value was determined from the maximal load exerted by the patient weight. Table 3.1 lists the material properties of cortical and cancellous bones chosen for simulation tests [PAR19].

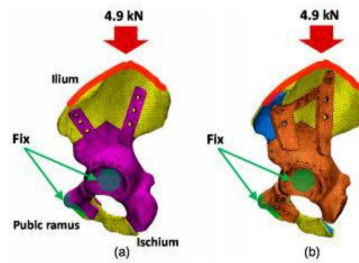


Fig. 3.3. Boundary conditions imposed onto the finite element model: (a) straight-type plates, (b) horseshoe-shaped plates [PAR19]

Table 3.1 – Material properties used for finite element simulation [PAR19]

Material	Density (g/cm ³)	Young's Modulus (MPa)	Poisson's Ratio (ν)	Tensile Strength (MPa)	Compressive Strength (MPa)
Cortical bone	1.64	16,700	0.26	106	157
Cancellous bone	0.16	155	0.30	6	6
Ti-6Al-4V	4.62	96,000	0.36	1070	1070

Fig. 3.4 presents the distribution of the von Mises stress in the case of straight-type plates and horseshoe-shaped plates. One may notice in the iliac fixation area a high-stress region and in the other parts, while in the pubic ramus and ischium fixation areas one may notice low-stress regions. For straight type plates the stress concentration in ilium, pubic ramus and ischium were 17.8%, 2.3% and 0.5%. For horseshoe-shaped plates the stress concentrations, for the same areas, were 19.8%, 2.3% and 0.6%. The maximal stress was 21% lower in horseshoe-shaped plates (38.6 MPa) than in straight-type plates (48.9 MPa) [PAR19].

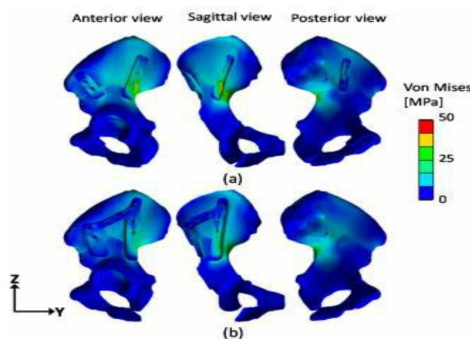


Fig. 3.4. Distribution of the von Mises stress: (a) straight type plates, (b) the horseshoe-shaped plates [PAR19]

Based on the stress analysis, the researchers concluded that the iliac fixation area carries the higher compression load. Thus, the ilium needed more stable fixation on implant, than the pubis and ischium areas. The horseshoe-shaped plates provided a more stable fixation in the pelvic implant.

Starting from these results, a finite element analysis was performed at the Manufacturing Engineering Department (Faculty of Machine Building - Technical University of Cluj-Napoca) regarding a pelvic implant to be made by 3D Printing. In this research, the Finite Element Analysis was performed to compare the results obtained by testing the porous structure samples and the results obtained from simulations. The simulation of the pelvic bone was done considering the characteristics obtained in the simulation of circular porous structure samples. The Finite Element Analysis process was based on the introduction of displacements on the 3D CAD model samples to obtain the specific mechanical properties, using the results of mechanical tests that were performed for compression in the case of samples made by 3D printing. After performing the mechanical tests of the porous structure samples, the structure that obtained the best results in terms of mechanical behavior was chosen, this being the circular porous structure. In order to solve the pelvic bone simulation, the characteristics of the circular porous structure have been preserved, being able to develop in the future an implant with this porous structure integrated within the bone structure.

Fig. 3.5 shows the manufacturing printing process of porous structures samples, process that was performed in the Laboratory Printing within the Faculty of Machine Building, University of Cluj-Napoca.

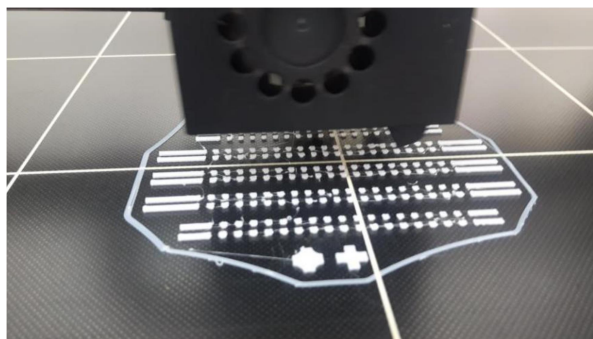


Fig. 3.5. 3D printing process

The parts were removed from the technological supports using different tools, like knives, scissors, tweezers etc. Fig. 3.6 shows samples of printed porous structures used for compression test: A-circular porous structure, B-square porous structure. Fig. 3.7 presents the sample used for flexural/bending and tensile tests: A-circular porous structure for the flexural test, B-square porous structure for flexural tests, C-circular porous structure for tensile tests, and D-square porous structure for tensile tests. The mechanical tests were performed using an Instron 3366 10 KN testing machine available in the Mechanical Testing Laboratory of Technical University of Cluj-Napoca.



Fig. 3.6. Printed samples made by FDM for compressive tests: A-circular porous structure, B-square porous structure



Fig. 3.7. Printed samples made by FDM: A-circular porous structure for flexural tests, B-square porous structure for flexural tests, C-circular porous structure for tensile tests, and D-square porous structure for tensile test

The properties of these types of structure subjected to compression, flexural and tensile loads were obtained from the mechanical tests. The average results of the external loads for different structures were considered in the finite element analyses.

The finite element analysis was performed according to the flowchart presented in Fig. 3.8. The ANSYS program was used to perform the simulations because it is one of the most used and complex simulation programs.

This project has been funded with support from the European Commission. This publication [communication] reflects the views only of the authors, and the Commission cannot be held responsible for any use which may be made of the information contained therein.

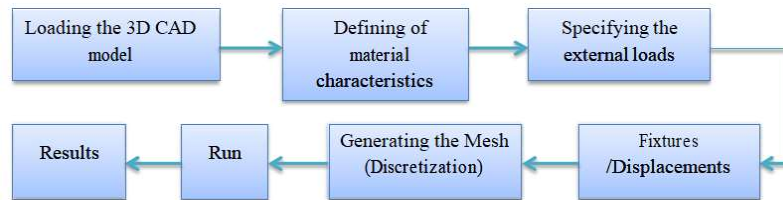


Fig. 3.8. Flowchart of the finite element simulation process

1. Importing the 3D CAD model: this is the first step in Simulation process. After loading the model, the name of the study and the type of study are specified. In this case a static analysis of the pelvic bone was performed. The pelvic bone model is presented in Fig. 3.9 as imported in *.stl format.
- 2.

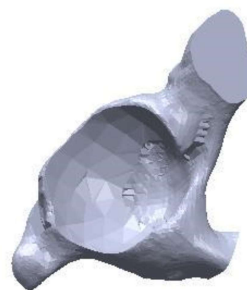


Fig. 3.9. 3D CAD model of the pelvic bone

3. Defining the material characteristics: the PLA material properties were defined in this stage as shown in Fig. 3.10. The properties of PLA are listed in Table 3.1. PLA has the density 1250 kg m^{-3} , Young's modulus 1371.5 MPa , Poisson's ratio 0.39 , and the tensile strength 33.81 MPa . A new material for bone simulation was then defined, with the specific characteristics of circular porous structure. The properties of the new material are presented in Fig. 3.11.

Table 3.1. PLA material properties [WWW03]

PLA Material Properties			
Melt temperature	Density	Tensile strength	Young's Modulus
150 - 220 °C	1.25 g/	14-117 MPa	2.7-16 GPa

This project has been funded with support from the European Commission. This publication [communication] reflects the views only of the authors, and the Commission cannot be held responsible for any use which may be made of the information contained therein.

Properties of Outline Row 4: PLA			
	A	B	C
1	Property	Value	Unit
2	Density	1250	kg m ⁻³
3	Isotropic Elasticity		
4	Derive from	Young's Modulus and Poisso...	
5	Young's Modulus	1371,5	MPa
6	Poisson's Ratio	0,39	
7	Bulk Modulus	2,078E+09	Pa
8	Shear Modulus	4,9333E+08	Pa
9	Field Variables		
10	Temperature	Yes	
11	Shear Angle	No	
12	Degradation Factor	No	
13	Tensile Yield Strength	33,81	MPa

Fig. 3.10. PLA material properties introduced in ANSYS

Properties of Outline Row 3: Os-cortical			
	A	B	
1	Property	Value	
2	Density	1600	kg
3	Orthotropic Elasticity		
4	Young's Modulus X direction	1,093E+10	Pa
5	Young's Modulus Y direction	1,478E+10	Pa
6	Young's Modulus Z direction	1,889E+10	Pa
7	Poisson's Ratio XY	0,276	
8	Poisson's Ratio YZ	0,501	
9	Poisson's Ratio XZ	0,28	
10	Shear Modulus XY	4,24E+09	Pa
11	Shear Modulus YZ	5,13E+09	Pa
12	Shear Modulus XZ	6,27E+09	Pa
13	Field Variables		
14	Temperature	Yes	
15	Shear Angle	No	

Fig. 3.11. Pelvic bone material properties introduced in ANSYS

- Specifying the external loads: at this stage, a force of 8000 N was applied to the bone as one may notice in Fig. 3.12. The force was applied from the upper part of the pelvic bone because in that area the force is also exerted. This force is 8 times the body weight and is considered the case of a person of 80 kg who climbs stairs and suddenly steps next to the stairs, causing a shock. The force of 8000 N was taken to obtain the mechanical results of the pelvic bone subjected to a shock. This force acting on the pelvic bone has three components: 1400 N, 800 N and -7840 N.

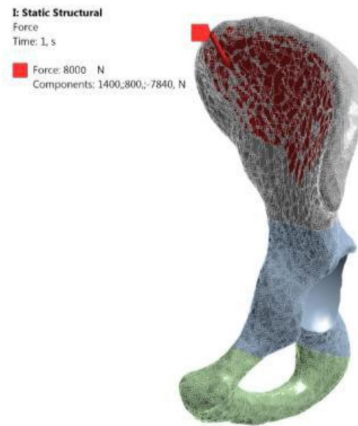


Fig. 3.12. Force applied to the pelvic bone

5. Fixtures/Displacements: in this stage the movement restrictions were imposed onto the finite element model. As one may notice in Fig. 3.13, displacement constraints were applied on the superior part of the bone. The displacement constraints were applied along two directions because, according to the anatomy of pelvic presented in Fig. 3.1, there are the areas where the pelvic bone comes into contact with the spine and form the entire pelvic area.

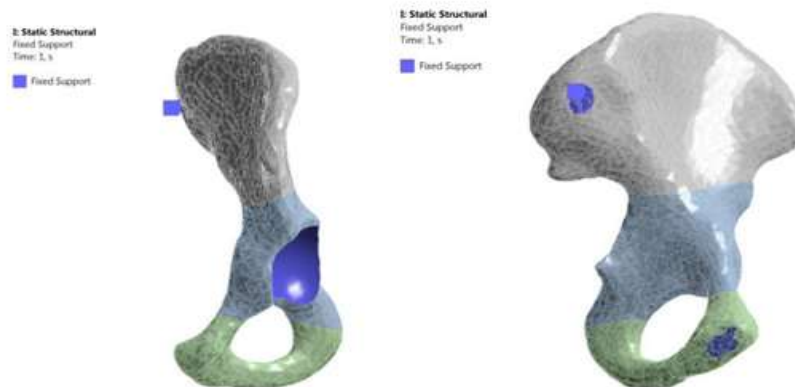


Fig. 3.13. Application of fixed supports on the pelvic bone model

6. Discretization: in this stage the finite element mesh was generated with the help of the program, using the Mesh command. Fig. 3.14 presents the details of the mesh.

This project has been funded with support from the European Commission. This publication [communication] reflects the views only of the authors, and the Commission cannot be held responsible for any use which may be made of the information contained therein.

Discretization means filling the analysis domain with finite elements and it is an automated and incorporated command in FEM program. Tetrahedral elements were used to generate the finite element mesh and the number of elements is 165779. Fig. 3.15 shows the mesh of the pelvic bone.

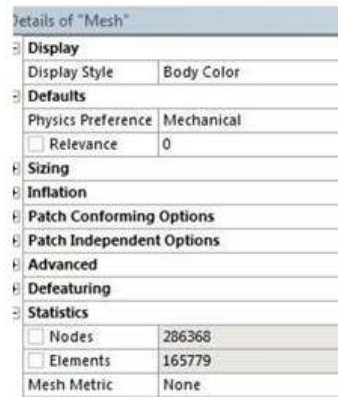


Fig. 3.14. Details of the finite element mesh



Fig. 3.15. Mesh generated in the case of the pelvic bone

7. Run: this function has the role of solving the set of algebraic equations, which are behind the mesh, in order to determine the mechanical response of the part.
8. Results: in this last stage the results of the static analysis are displayed. In this case, the results for Equivalent Stress (von-Mises) and Total Deformation were analyzed. Fig. 3.16 a and b show the distributions of the equivalent stress and total deformation, respectively.

This project has been funded with support from the European Commission. This publication [communication] reflects the views only of the authors, and the Commission cannot be held responsible for any use which may be made of the information contained therein.

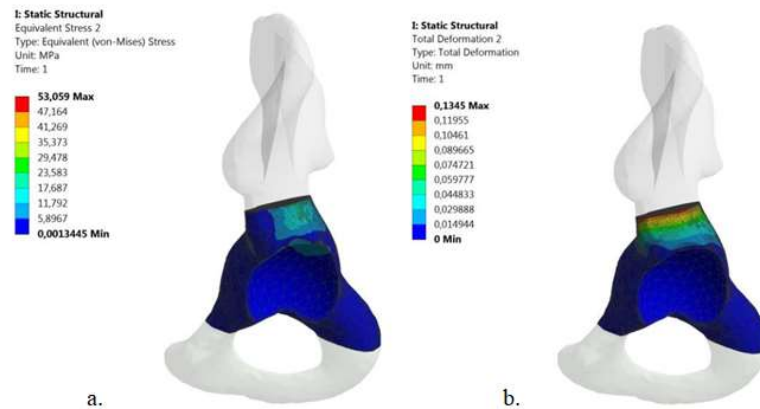


Fig. 3.16. a) Equivalent stress results; b) Total deformation results

Representative colored areas can be observed in Fig. 3.16.a for each value of the equivalent (von Mises) stress. The area of interest of this research is highlighted by different shades of blue. As one may notice, the color dark blue predominates, which highlights the fact that the equivalent stress is minimal in those areas with a value of 0.0013445 MPa. In the areas indicated with a lighter blue the equivalent stress increases and has the values between 5.8967 MPa and 17.678 MPa. This area indicated by a lighter blue color is the contact area with the acetabular cup and femur bone, which creates higher stresses in those regions. On the edges of the contact area with the acetabular cup, light shades of orange and red can be observed, which indicate a higher, almost maximum equivalent stress with values between 41.269 MPa and 53.059 MPa.

As previously presented in the research realized by the Orthopaedic Oncology Clinic, Specific Organs Center Branch, National Cancer Center, in Korea, the biomechanics of a plate introduced in a 3D printed pelvic implant was investigated using FEA. In this research, a distributed load of 4.9 KN was applied to the pelvic bone. According to [PAR19], the maximum value of the equivalent (von Mises) stress is 50 MPa in this case.

Comparing the results obtained in the previous research and the results of the simulation performed above, there are closed values, which indicate that these results may be realistic in the case of a pelvic bone. The contact area with the trabecular bone does not have high values of the equivalent stress. These results help develop implants that can replace a destroyed pelvic area.

This project has been funded with support from the European Commission. This publication [communication] reflects the views only of the authors, and the Commission cannot be held responsible for any use which may be made of the information contained therein.

In the case of Total Deformation, the area where higher values appear is the upper area of the interest pelvic bone. The area indicated with dark blue color corresponds to zero deformation. The upper area of the pelvic bone corresponds to the the maximum total deformation with a value of 0.1345 mm. As one may notice in fig. 3.16.b, in other areas the total deformation values are between 0.014944 mm and 0.11955 mm.

In the case of a research realized at the Department of Orthopaedics Surgery and Department of Radiology, The Second Affiliated Hospital and Yuying Children's Hospital of Wenzhou Medical University, China, a finite element analysis of the entire pelvic was performed. In this case, a force of 600 N was applied on the pelvic bone. The ANSYS program was used and the total deformation of the entire pelvic was determined. Fig. 3.17 shows the results obtained in this research. One may notice that the area of maximum total deformation is in the middle of the pelvis, the maximum value being 0.08002 mm [CAI20].

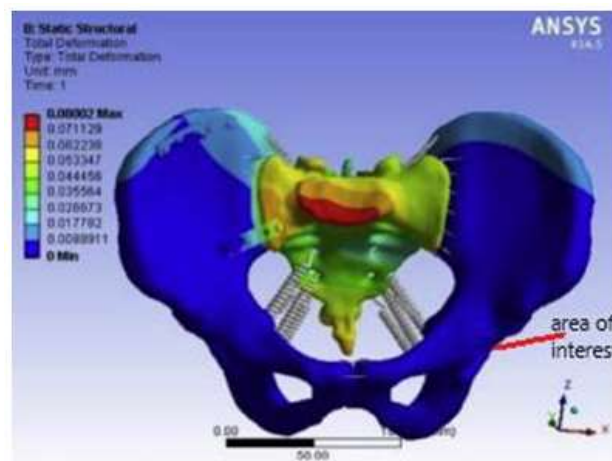


Fig. 3.17. Total Deformation results from finite element simulation [CAI20]

One may also notice in Fig. 3.17 that the area of interest for this research, more exactly the area of contact with the trabecular bone (indicated in red), has very small total deformation (almost 0 mm). Thus, in this research the total deformation was determined only in the interest area, and, if one compares the results of the total deformation obtained in simulation with the total deformation from previous research, it can be seen that the values are close and tend to 0 mm.

Comparing the results obtained in the research presented at the Department of Orthopaedics Surgery and Department of Radiology, the Second Affiliated Hospital and

Yuying Children's Hospital of Wenzhou Medical University, China with the results obtained after the testing realized at the Technical University of Cluj-Napoca, a difference can be observed. The densities have close values, 1.60 g/cm^3 and 1.64 g/cm^3 , respectively. The Young's modulus has a low value in the case of pelvic bone (14.860 MPa) as compared to the cortical bone (16.700 MPa). The research was done on cortical bone involved the entire cortical bone with support rods. In the simulation testing and simulation performed in the case of pelvic bone, only the contact area between the pelvic bone and acetabular cup was taken into account. In this sense the tensile strength and compressive strength have lower values, 21.49 MPa and 30.81 MPa , respectively, in comparison with the cortical bone which presents values of 106 MPa and 157 MPa (see Table 3.2).

Table 3.2. Comparison between the pelvic bone and the cortical bone

	Density (g/cm^3)	Young's Modulus (MPa)	Poisson's Ratio	Tensile Strength (MPa)	Compressive Strength (MPa)
Pelvic bone	1.60	14.860	0.35	21.49	33.81
Cortical bone	1.64	16.700	0.26	106	157

In conclusion, the Finite Element Analysis was performed in the case of pelvic bone. The characteristics of circular porous structure were used, this structure presenting better mechanical characteristics than square porous samples.

The analysis was performed by introducing the force of 8000 N , which is the equivalent of a person of 80 kg and suffer from a severe shock caused by a fall or accident, and obtaining the equivalent stress and total deformation. The results showed that the bone has an equivalent stress average value of 17.678 MPa . There were also areas where the equivalent stress was higher with value around 35.373 MPa . In the case of the equivalent stress, the results are close to the results obtained in other research which indicates that the values are closed to the real ones.

The total deformation presents values between 0 mm and 0.1345 mm . In the contact area with an acetabular cup the total deformation is 0 mm , which shows that in that area the bone does not deform. In the case of total deformation, the results are close to the ones reported by other researchers, which shows that the values are close to the real ones in this case as well.

The manufacturing of the bone was realized as in the case of porous structure samples. The 3D printing procedure used for manufacturing was Fused Deposition Modeling (FDM) from PLA material filament. The FDM equipment created the bone by continuously depositing layers of heated material. For the manufacturing process, the same Leapfrog Creatr HS 3D printing machine was used. Fig. 3.18 shows the printed pelvic bone made from PLA filament.



Fig. 3.18. 3D printed model of the pelvic bone

3.3. Design study of anatomically shaped lattice scaffolds for the bone tissue recovery

3.3.1. Introduction

Tissue scaffold, or just scaffold, is a highly porous medical implant that is applied as a support for growing a missing part of tissue from stem cells. It is often used in tissue engineering, when the volume of the tissue, missing because of an accident or a disease, is too large for the tissue to be spontaneously regenerated. Here we focus on design of bone scaffolds, using a lattice type scaffold as an example.

Major scaffold design concepts for bone tissue recovery are characterized by labyrinthine design. Their main shortcomings are low level of permeability for new growing tissue, poor design adaptability regarding particular anatomy and required biomechanical conditions during recovery, as well as very demanding post processing after fabrication by

This project has been funded with support from the European Commission. This publication [communication] reflects the views only of the authors, and the Commission cannot be held responsible for any use which may be made of the information contained therein.

additive technologies. In contrast to most of the existing solutions, latticed scaffold design does not try to imitate the trabecular structure and rejects the labyrinthine concept. It is characterized by simple 3D latticed support structure, which provides a high level of permeability for the new growing tissue cells, and at the same time a proper level of bio-adhesiveness. In addition, its design is easy to manage in order to make it follow the particular anatomical shape and to provide the required elastic properties and structural strength.

This chapter presents a part of design concept proving process, which involves stress analysis of the scaffold that is anatomically shaped to the upper part of proximal diaphyseal trauma of rabbit tibia. The aim of the analysis was to identify functional relations between design parameters and elastic properties of the scaffold, which may be used to get the optimal values of elastic properties of the scaffold for a specific trauma-fixation case. The design study shown in the paper was done for the case of lattice scaffold anatomically shaped to the upper part of proximal diaphyseal trauma of rabbit tibia.

3.3.2. Lattice scaffold design concept

Anatomically shaped lattice scaffold (ASLS), developed at University of Nis, Faculty of Mechanical Engineering [STO13], [MIL15], [KOR16], consists of two groups of simple struts (Fig. 3.19). The struts in the first group follow the geometry of outer wrapping surface of the bone but they also follow the geometry of inner wrapping surface (near the medullary cavity). These *wrapping struts* form outer and inner surrounding support of the latticelike structure, which is characterized by densely interlaced lattice. Yet, this wrapping lattice is still sparse enough to enable easy penetration of vascular and nerve tissue/structures/ to the interior of the bone graft, ensuring the preconditions for bone tissue growth. The struts of the second group are located in the space of (future) spongy bone and they connect wrapping lattice structures providing required strength of the scaffold as a whole. This group is called *inner structure of cross-linking struts* and it is characterized by sparsely interlaced lattice than wrapping ones. Low density of the inner structure is designed to assure easier and deeper vascularization and innervation of the bone graft (Fig. 3.20.a).



Fig. 3.19. Design concept of ASLS (Anatomically Shaped Lattice Scaffold) [STO13]

A very important feature of the ASLS design is its ability to withstand a certain component of the mechanical load that is required to convey by the traumatized bone, in order to keep ossification process within the bone graft active (Fig. 3.20.b). Main component of the mechanical load will be transferred via fixation structure. This requirement imposes optimization of the ASLS design according to the trauma and fixation case and consequently in regard to the load that ASLS has to withstand (Fig. 3.20.b). The goal of this optimization is to adjust the stiffness of the scaffold to match the stiffness of the surrounding bone, in order for the load on the non-traumatized part of the bone to remain the same as before the trauma. If the scaffold is too flexible, the load on the bone may be too high, and if the scaffold is too stiff, the contact pressure between the scaffold and the bone may be too high. In both cases, further bone trauma may occur.

3.3.3. CAD models

Two models of ASLS were designed, to match the anatomical shape of the upper part of proximal diaphyseal trauma of rabbit tibia (Fig. 3.21). The first model was designed to wrap the whole bone's tube in the defect region (Fig. 3.22). The main purpose of this model (from now on referred to as „fully wrapped scaffold”), was to study the sensitivity of elastic properties of lattice design to change of principal design parameters. Compared to usual scale of the defect found in orthopaedic practice, this scaffold model may be considered too large and unfeasible. The second model, showed in Fig. 3.23, is congruent to the realistic shape of bone defect (Fig. 3.21), and is based on CT images of rabbit tibia. This model was subjected to a load case that approximately represents physiological loading after the

This project has been funded with support from the European Commission. This publication [communication] reflects the views only of the authors, and the Commission cannot be held responsible for any use which may be made of the information contained therein.

surgery. Then, the sensitivity study similar to the first one was performed, in which the struts angle was changed, and the response of bone-scaffold assembly obtained.

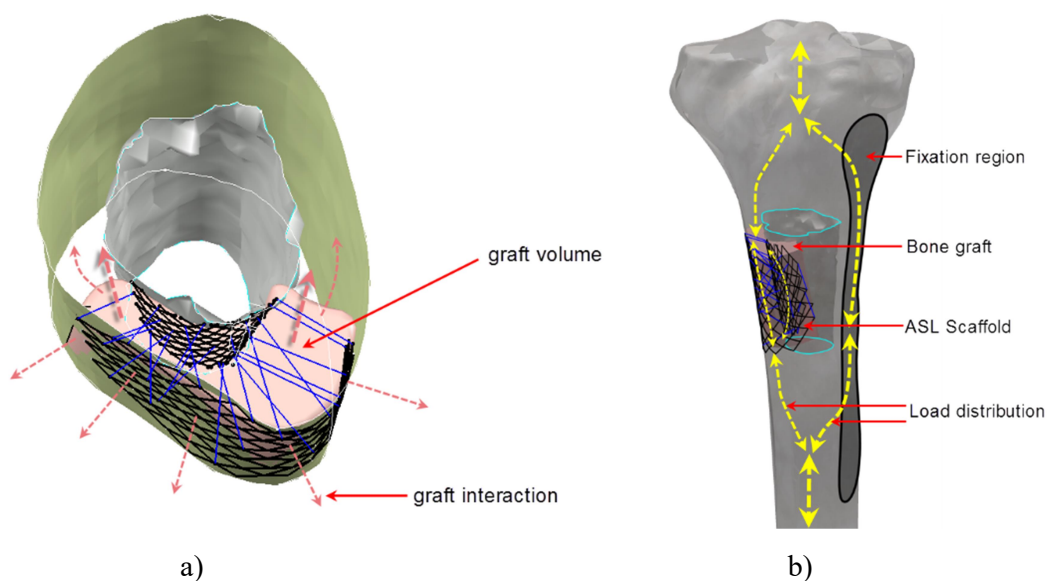


Fig. 3.20. Bone graft insertion (a) and load distribution schema (b) [STO13]

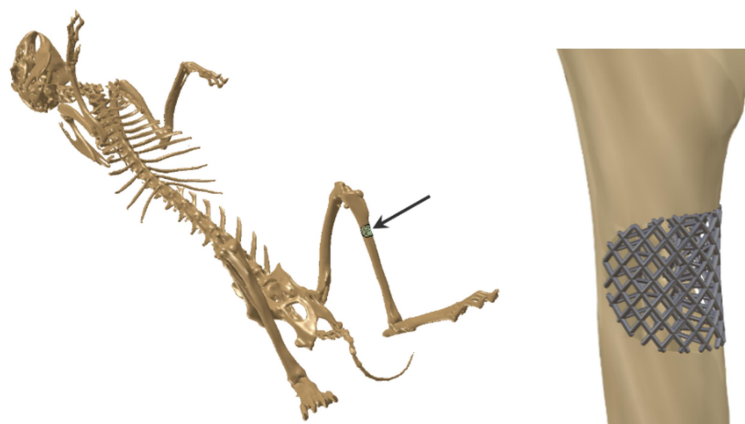


Fig. 3.21. ASLS for proximal diaphyseal trauma of rabbit tibia [STO13]

This project has been funded with support from the European Commission. This publication [communication] reflects the views only of the authors, and the Commission cannot be held responsible for any use which may be made of the information contained therein.



Fig. 3.22. ASLS for complete envelopment of the bone – fully wrapped ASLS [STO13]

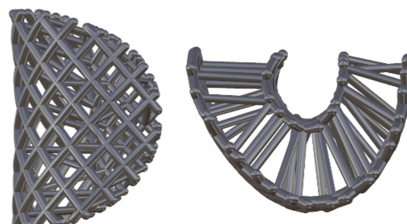


Fig 3.23. ASLS for realistic bone defect (D = 8m) [STO13]

3.3.4. Sensitivity study of fully wrapped ASLS design elastic properties to principal parameters changes

In order to study the sensitivity of elastic properties of *fully wrapped* ASLS design (Fig. 3.22) to variations of major design parameters, a finite element model was built and positioned between two very stiff cylindrical bodies with parallel inner surfaces. It was then subjected to axial compression, with the force acting on one of the surfaces, the other one being fixed. Frictionless contact was defined between the scaffold and two other bodies. Such boundary conditions have been chosen to minimize their effect on scaffold deformation, so that the changes in stress-strain field may be correlated only to changes in principal design parameters. The values of three different design parameters (density of the struts, lattice's struts cross-sectional area and angle of struts intersection) were changed during the study. In this way, a total of seven scaffold instances, driven by parameters values given in Table , were created (Fig. 3.24).

Table 3.3. Fully wrapped ASLS instances used in the study and corresponding parameters [STO13]

Instance No.	Struts density [mm ⁻¹]	Struts diameter [mm]	Struts cross-sectional area [mm ²]	Struts angle [°]	Struts effective volume [mm ³]	Porosity
1	0.67	0.4	0.16	52	56.31	0.885
2	0.53	0.4	0.16	52	46.1236	0.906
3	0.43	0.4	0.16	52	36.7678	0.925
4	0.67	0.32	0.1024	52	38.94	0.921
5	0.67	0.48	0.23	52	80.42	0.836
6	0.67	0.4	0.16	32	53.2	0.892
7	0.67	0.4	0.16	72	55.82	0.886

This project has been funded with support from the European Commission. This publication [communication] reflects the views only of the authors, and the Commission cannot be held responsible for any use which may be made of the information contained therein.

Scaffold porosity, defined according to Eq. (3.1), was also used, as derived parameter describing scaffold geometry.

$$\text{Scaffold porosity} = \left(1 - \frac{V_{str}}{V_{circumscribed}} \right) \times 100\% \quad (3.1)$$

where V_{str} is the effective volume of scaffold struts and $V_{circumscribed}$ is the volume of approximately cylindrical body circumscribing the scaffold (490.8 mm^3).

Maximal axial displacement u_x and maximal equivalent Von-Misses stress σ_{VM} were monitored as output quantities, as well as the structural stiffness K_S (Eq. 3.2) and structural modulus E_S (Eq. 3.3):

$$K_S = \frac{F}{\Delta l} \quad (3.2)$$

where F is the axial load and Δl is the change of initial scaffold length,

$$E_S = \frac{F \cdot l_0}{A \cdot \Delta l} \quad (3.3)$$

where l_0 is the initial scaffold length (10mm) and A is the area of the front surface of approximately cylindrical body circumscribing the scaffold (49.08 mm^2).

A linear elastic material model was used to represent the mechanical behavior of the scaffold. The scaffold was supposed to be built from Arcam Ti6Al4V titanium alloy, characterized by typical values of Young's modulus (120GPa), Poisson's ratio (0.36), yield strength (950MPa) and ultimate tensile strength (1020MPa). A hypothetic, extremely stiff, material was used to model the bodies between which the scaffold is pressed, with Young's modulus set to $1 \times 10^6 \text{ GPa}$. Each of FE model instances was meshed with 10 node quadratic tetrahedron elements, using average global edge length of 0.2mm. Depending on instance, mesh size varied from 47000 to 105000 elements. Finite element model of the fifth instance is shown in Fig. 3.25.

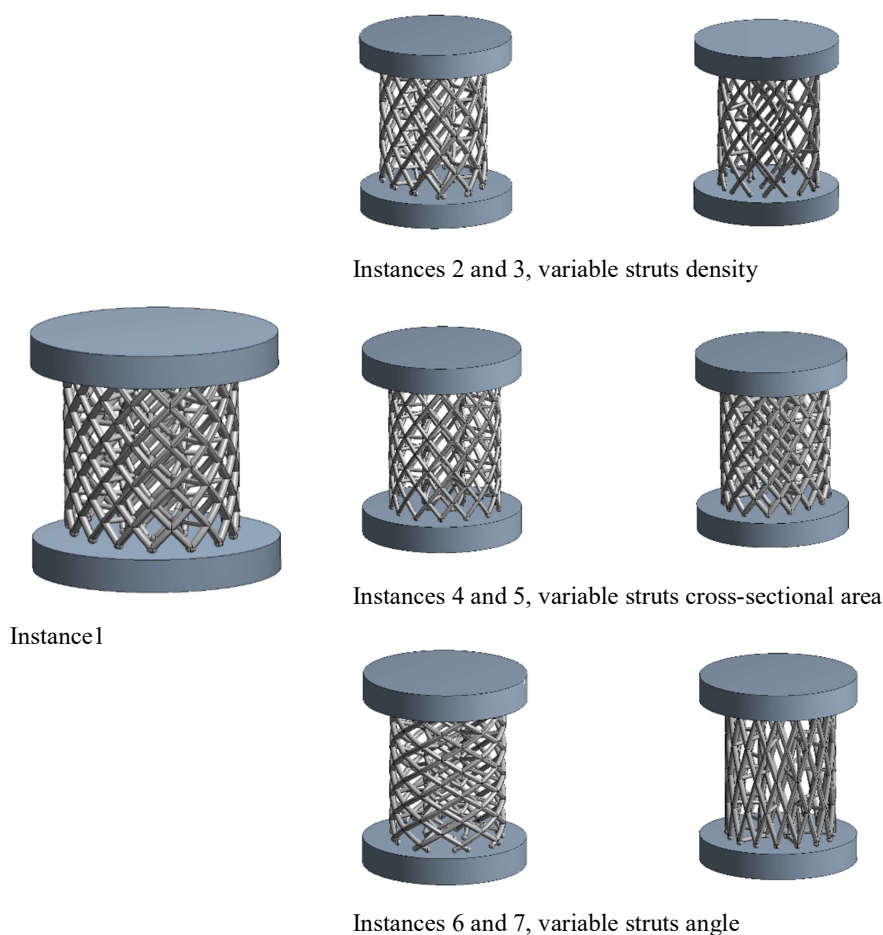


Fig.3.24. Instances of fully wrapped ASLS, obtained by change of principal design parameters [STO13]

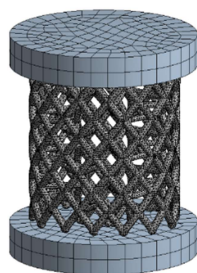


Fig. 3.25. Finite element model of fully wrapped ASLS [STO13]

Typical results of the analyses conducted within the study, are shown in Fig. 3.26. Maximal values of axial displacement and equivalent Von-Misses stress, as well as values of structural stiffness and structural elasticity, obtained numerically for all instances, are given in Table 3.4. Maximal values of stress in the scaffold are in all cases well below yield strength of titanium alloy (950MPa).

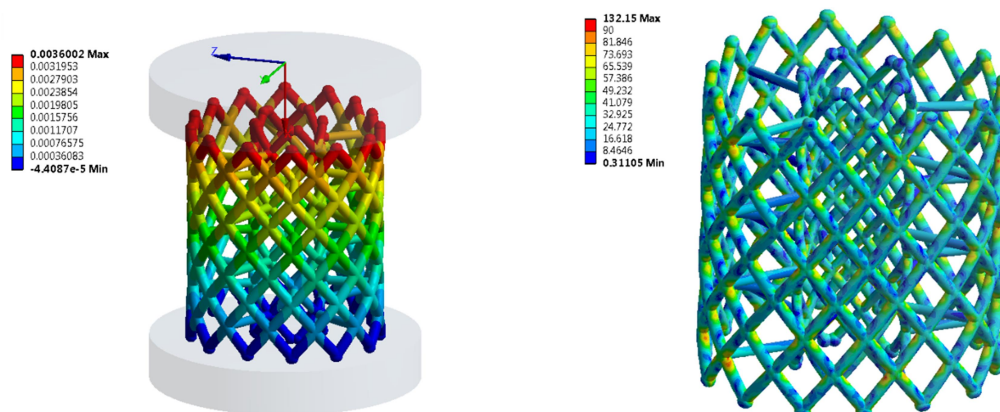


Fig.3.26. Resulting fields of axial displacement u_x and equivalent Von-Misses stress σ_{VM} , for instances 5 and 1 respectively [STO13]

Based on the complete set of results, sensitivity of structural stiffness and modulus to principal design parameters was estimated. Fig. 3.27 shows that a nearly linear correlation exists between struts density and structural modulus. Correlation between struts cross-section area and structural modulus is a bit further from linear one (Fig. 3.28), while the one between structural modulus and struts angle is noticeably nonlinear (Fig. 3.29).

Table 3.4. Output values resulting from design study of fully wrapped ASLS design and calculated quantities [STO13]

Instance No.	$u_{x \max}$ [mm]	K_S [N/mm]	E_S [N/mm ²]	$\sigma_{VM \max}$ [N/mm ²]
1	0.00703	8537.0	1739.4	132.15
2	0.01287	4662.8	950.0	217.25
3	0.02652	2262.1	460.9	350.46
4	0.01447	4145.5	844.6	230.16
5	0.00360	16665.9	3395.7	212.42
6	0.03614	1659.8	338.2	278.81
7	0.00282	21282.0	4336.2	63.42

This project has been funded with support from the European Commission. This publication [communication] reflects the views only of the authors, and the Commission cannot be held responsible for any use which may be made of the information contained therein.

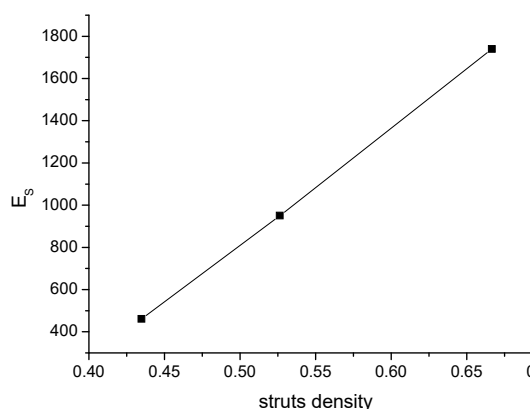


Fig. 3.27. Sensitivity of structural modulus E_s to change of struts density [STO13]

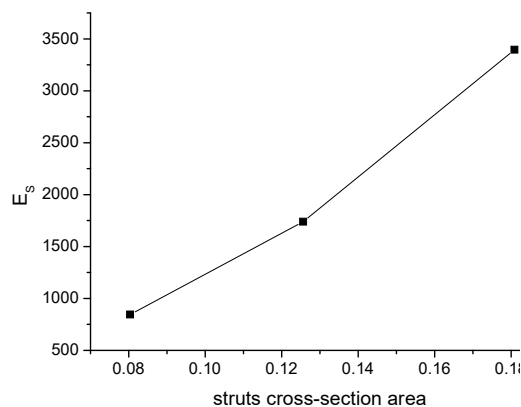


Fig.3.28 Sensitivity of structural modulus E_s to change of struts density [STO13]

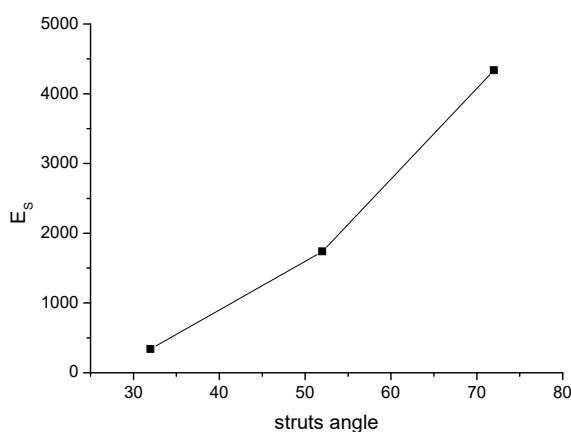


Fig.3.29. Sensitivity of structural modulus E_s to change of struts angle [STO13]

3.3.5. Sensitivity study of realistic shape lattice scaffold elastic properties to change of struts angle

Scaffold shape and loads are never as ideal as shown in previous study, in which they were deliberately simplified to explore the mechanical behavior of fully wrapped ASLS design. To get a step closer to reality, a more realistic scaffold was modeled and assembled with a model of rabbit tibia segment, based on CT images. Three assembly instances were created, with variable struts angle (Fig. 3.30).

This project has been funded with support from the European Commission. This publication [communication] reflects the views only of the authors, and the Commission cannot be held responsible for any use which may be made of the information contained therein.

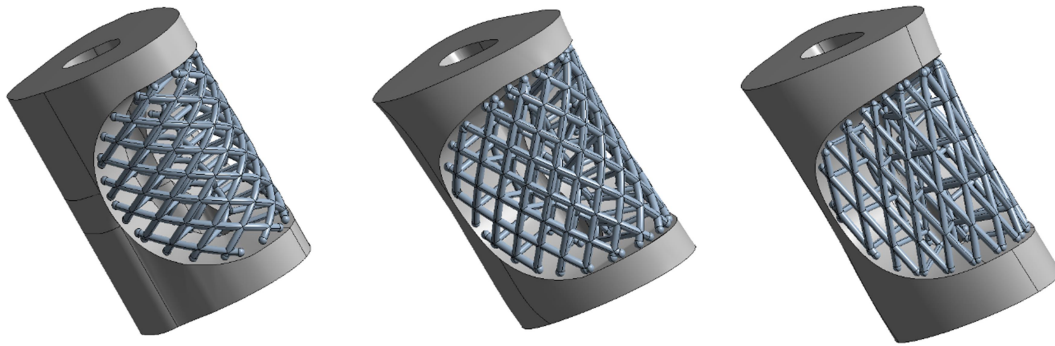


Fig.3.30. Three instances of bone segment-scaffold assembly, in which struts angle was modified to take representative values of 32° , 52° and 72° respectively [STO13]

Scaffold material was defined in the same way as in the previous study, and bone material was set to be linear elastic, characterized by mid value of Young's modulus reported in literature [AND10] for rabbit tibia (22GPa), typical reported Poisson's ratio (0.33) and ultimate tensile strength (195MPa). Fixation of the scaffold to the bone was approximated by bonded contact between neighboring surfaces of the two components. To approximate the axial load acting on the bone, one of the frontal surfaces of the bone was fixed, while equally distributed load of 60N was applied to the other (Fig. 3.31). Typical results of the analyses conducted within the study, are shown in Fig. 3.32 and Fig. 3.33.

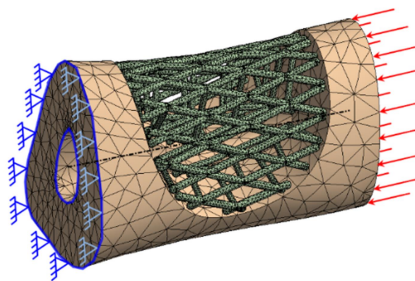


Fig. 3.31. Finite element model of bone segment-scaffold assembly. Boundary condition and load shown in the picture are defined on front surfaces of the bone segment [STO13]

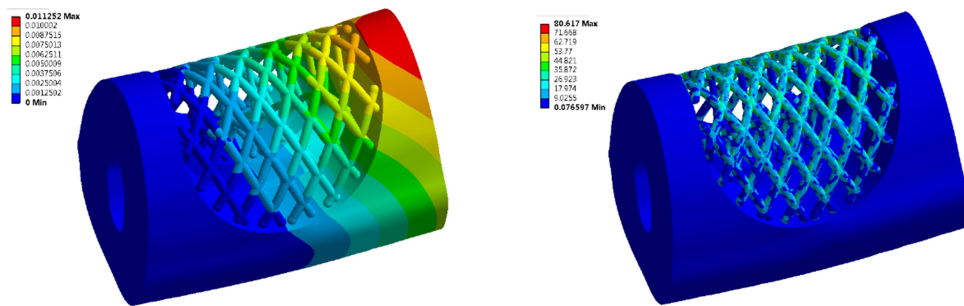


Fig. 3.32. Total deformation and equivalent stress field on bone segment - scaffold assembly.
Struts angle is set to 32° [STO13]

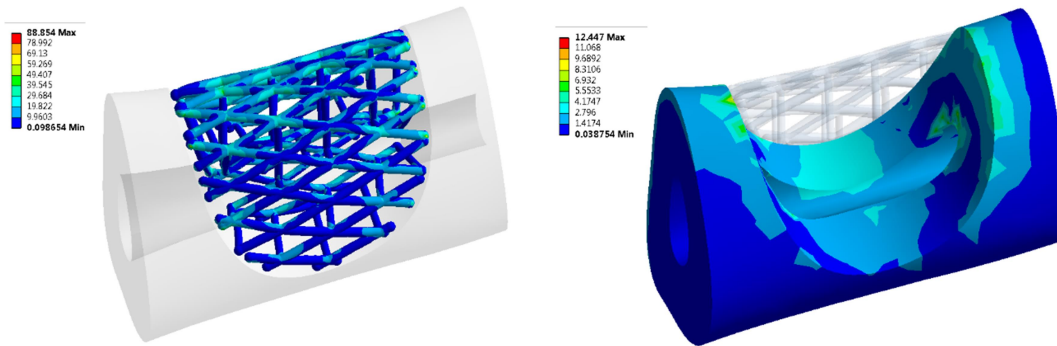


Fig. 3.33. Equivalent stress field on bone and scaffold shown separately. Struts angle is set to 72° [STO13]

From previous images it may be seen that maximum value of equivalent stress in the scaffold (88.8MPa at struts angle of 72°) is much lower than Yield strength of titanium alloy (950 MPa). The same is true for maximal stress in the bone (12.5 MPa at struts angle of 72°), which is well below ultimate bone strength (195 MPa). Correlation between struts angle and defect length dilatation obtained during the study is shown in Fig. 3.34.

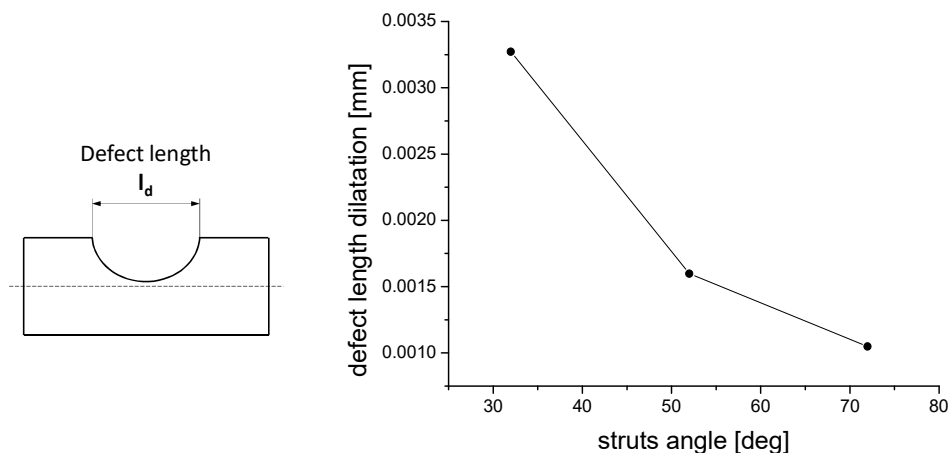


Fig. 3.34. Bone defect length dilatation vs. struts angle [STO13]

3.3.6. Production using additive manufacturing technologies

The scaffold featured in second study was produced by additive manufacturing technologies, namely Electron Beam Melting (EBM) and direct metal laser sintering (DMLS) and implanted in-vivo into rabbit tibia to observe the successfulness of bone healing process (Fig. 3.35) [MIL20]. Mechanical testing, to verify the analysis results, should be a part of the future research.

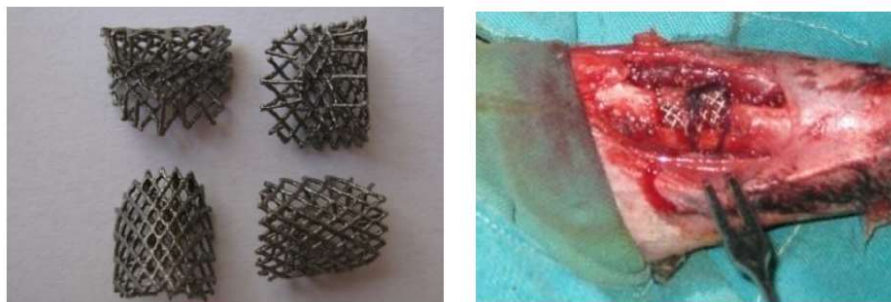


Fig. 3.35. ASLS produced by additive manufacturing technologies (left), ASLS implantation into rabbit tibia (right) [MIL20]

This project has been funded with support from the European Commission. This publication [communication] reflects the views only of the authors, and the Commission cannot be held responsible for any use which may be made of the information contained therein.

3.3.7. Conclusions

Design study described in the paper showed that the design concept of *anatomically shaped lattice scaffold* enables the easy control of scaffold's stiffness by changing the three main design parameters: density of the struts, cross-sectional area of the struts and angle of struts intersection. Furthermore, the study helped to determine functional relationships between these three design parameters and mechanical properties of the scaffold structure. Knowing these dependencies, it is much easier to properly customize the design of ASLS and to pair it with a fixation frame, to ensure a proper load distribution between fixation and scaffold as well as to keep the ossification process active inside the bone graft. Thus, it may be concluded that customization of ASLS design to the anatomy of a traumatized piece of the bone as well as to the requested load distribution, improves tissue recovery.

From the study, it is obvious that struts angle is the design parameter which has a major influence on elastic properties of lattice scaffold. Moreover, the correlation between struts angle and structural stiffness of the scaffold is noticeably nonlinear, which is probably due to the fact that axial compression of the struts starts to dominate over other deformation modes as struts direction gets closer to load axis (in this case at struts angle of 90°).

3.4. Mechanical behavior of a dynamically stressed customized skull implant made from different types of biomaterials by SLS and vacuum casting methods

The aim of this study was to determine the behavior of the customized implant, considered as being assembled inside a living patient, being surrounded by “living” neighboring areas, in the context when the medical implant is realized from different types of materials, with different shape variations and stressed in the same dynamical conditions. For a virtual evaluation of such a hypothesis the ANSYS finite element analysis program was chosen, which allows the construction and running of different types of projects that may include practically any type of possible stress that can be considered for such an implant. The experimental project that has been designed consists in striking a customized implant, in

assembly state, with a gravitational pendulum. The pendulum consists of a steel ball having a diameter of 100 mm and the weight of 4.11 kg, the length of its string being 1000 mm. The initial position of the pendulum string is horizontal, parallel with the terrain, travelling then by free falling, before the impact with an angle of 90 degrees in total. The velocity of the pendulum at the impact moment was determined by using the energy conservation law and had a value of 4.47 m/s.

Three virtual models were considered for the realized, their geometry being defined in a CAD format that it is accepted and recognized by the ANSYS finite element analysis program. The model of representing the ball pendulum has not been difficult to achieve, due to the fact that it was virtually generated by using the SolidWorks CAD program, the model being easily converted in any CAD format required for the made analysis. The model of the customized implant was realized by using a CAD system as well, by not using boolean operations, being possible to be represented in any format that is required for the made analysis. The model of the destroyed area consists in a native medical model which was obtained by processing the data collected from a Computer Tomograph, its representation in “stl” format being simple and easily realized with a dedicated software - MIMICS [WWW04], software which was specially designed for processing medical models. The “stl” model being not adequate to the aim that has been defined, there were several trials performed during our studies in order to convert the model in a format that is acceptable for the proposed assessment, using some particular CAD programs that are commercially available. The obtained results proved to be unusable at the end, in all cases, the converted files having very high dimensions (hundreds of MB). The use of Geomatic Studio program was a reliable choice in this case, due to the fact that this program allowed obtaining reliable results at the end, even if the resulted models were represented only by an approximation of the initial “stl” models that were used for the made analysis. With the aim of simplifying the model structure to be analyzed, the model that resulted from the processing of the data taken from the Computer Tomograph (an “stl” model of a skull implant) was “cut”, by using the MAGICS program, the resulted model containing at the end the destroyed area and just a small area of the skull structure that is surrounding the destroyed area. This decrease of the model is justified not only by its simplification in the assembly context, but also by the fact that in real applications, the single role of the model in the destroyed area is to check the shape of the implant to be realized. Figure 3.36 shows the stages that are required to be followed in order to realize the simplified model, with the observation that one stage is considered to be

adequately realized if at its end, the model results with no errors. The 3D model of periacetabular implant was designed using MIMICS software. In Fig. 3.37 there are presented the pelvic bone with grey color and the implant with yellow color. For fixing the implant in hip bone were designed straight-type plates and horseshoe-shaped plates, presented also in fig. 3.37.

By considering the way the final surface of the model is generated and built, it is easy to notice that the resulted surface is only an approximation of the initial model considered for the analysis. The errors which result in comparison with the initial model were determined by the overlapping the considered models (initial and final), the dimensional differences between the models being in terms of tenths of microns, the average errors being less than five hundreds of a micron. The model conversion (the approximation of the model) was considered as being adequate due to the fact that in the case of medical models, the dimensional errors are in the size of ± 1 micron, values that are considered acceptable in this case. The final validation of the model correctness was given by the finite element analysis program, the checking being validated by its possibility to recognize, import and meshing the respective model (Fig. 3.37). Once the CAD models of the components involved in the experiment were defined in an adequate manner, the next step consisted in the assembly generation which was made using the Assembly module of the SolidWorks program (Fig. 3.38).

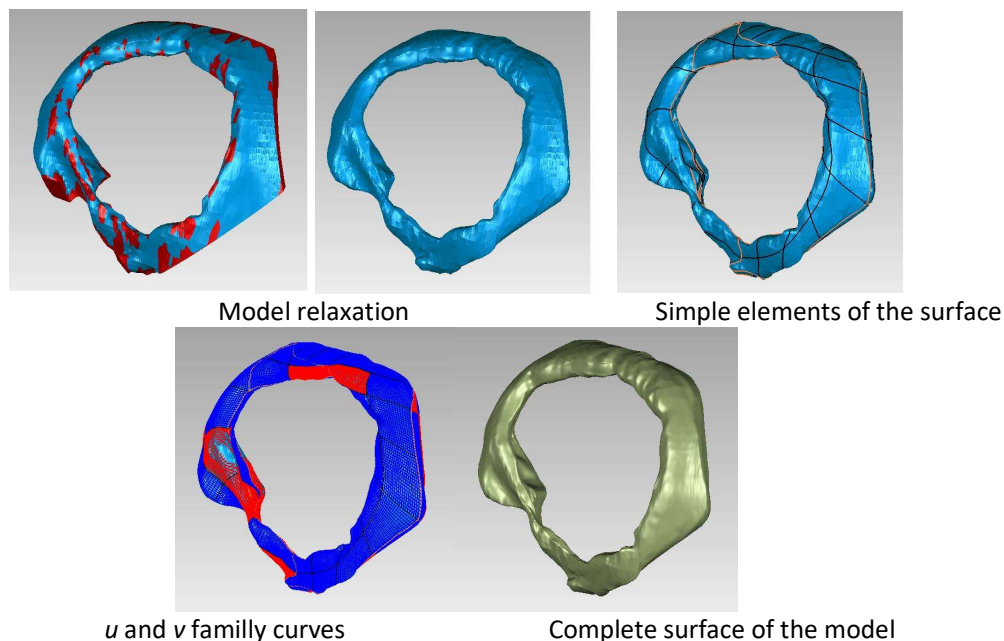


Fig. 3.36. Main stages required for the conversions of an “stl” model into a CAD model

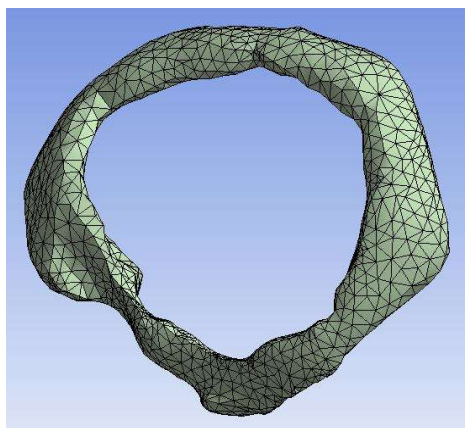


Fig. 3.37. Model validation

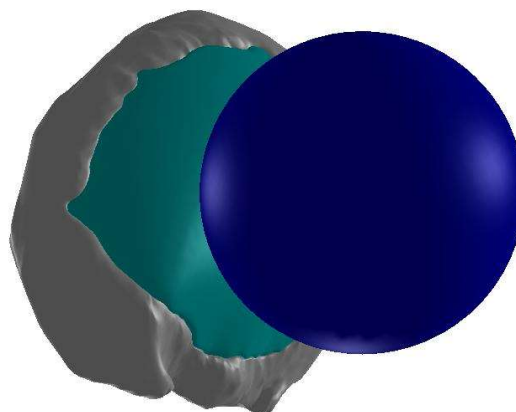


Fig. 3.38. Generated assembly

In the stage of defining the models there were considered the options of the ANSYS program regarding the stiffness of all the models involved in the experiment. In this sense, in the case of the ball it was selected the Rigid option and for the destroyed area and the customized implant was selected the Flexible option.

This project has been funded with support from the European Commission. This publication [communication] reflects the views only of the authors, and the Commission cannot be held responsible for any use which may be made of the information contained therein.

- The ball of the pendulum was considered as being rigid, the maximum dimension of a discretized element being limited to 50 mm. Of course, such a high value, as compared with the size dimensions of the ball has not been used in the case of any other finite element, these elements having variable size, much lower in size and established in close connection with the conditions imposed regarding the approximation accuracy of the shape and the surface quality. By considering that the ball has been defined as being a rigid element, the high value of the size for the elements to be discretized in the case of the ball do not have a significant influence on the accuracy of the obtained results. On the other hand, the large dimension of these finite elements shortens the computation time, due to the lower number of nodes, requiring complex successive calculus for their positions at every stage of the analysis.
- The destroyed area and the customized implant were considered as being flexible elements, the determination of the way of deforming and the stresses accumulated in these components being one of the main objectives of the simulation. The maximum size of the finite elements was maintained at default values, very restrictive conditions being imposed regarding the accuracy of model approximation and the surface quality of these elements.

Figure 3.39 shows the final and adequate shape of the discretized assembly, with respect to the conditions that were previously detailed.

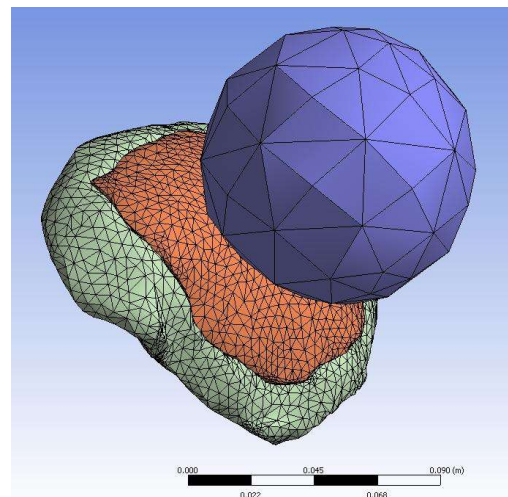


Fig. 3.39. Meshed assembly

This project has been funded with support from the European Commission. This publication [communication] reflects the views only of the authors, and the Commission cannot be held responsible for any use which may be made of the information contained therein.

In the experiment that was conceived and presented previously, the materials which are involved in the analysis are the human bone, the material from which the implant is made and the material of the ball pendulum.

a) Ball. The material of the ball is common steel, the mechanical properties of the material being not important from the experimental point of view, due to the fact that after the analysis, the stresses are not evaluated in the ball, but only the effects of the striking of the ball against the implant – destroyed area assembly region. The only characteristic which is important in this case is the weight of the ball (4.11 kg), this property defining its dynamical characteristics.

b) Human bone. Most of human bones are represented by a complex natural structure which consists of an external dense and compacted layer, namely the compacted bone or cortical bone and a porous core, which is represented by the trabecular zone. The bone material is a composite material that consists in a mixture of collagen and hydroxylapatite. The crystal apatite is very rigid and resistant. Young's modulus of these crystals is 165 GPa, this value being comparable to the one of steel (200 GPa). The collagen does not respect precisely Hooke's law, its Young modulus being in this case about 1.24 GPa. The Young's modulus of the assembly is 17 GPa, this value being an intermediate value of the apatite and the collagen. Like in the case of any composite material with high quality, the strength of the bone is higher as compared to the elements from its composition (separately considered), its properties being improved due to the fact that by the soft component (collagen) the stiffness is being decreased and the occurrence of the small cracks caused by the fragility of the bone is prevented, while the rigid component (apatite) is maintaining the shape of the assembly in a compacted state [FUN93].

Research that was made in this field indicates that the bone tissue is an orthotropic material, its anisotropy being given by the flat shape of the hydroxylapatite crystals and their partial alignment in a direction considered as being longitudinal, direction which determined the most rigid and most stress-resistant direction of the material [WWW04]. If the bone is dry, the Young's modulus increases and the yield strength and fracture strength decrease due to the fact that the content of the collagen is also decreased. A bone which is completely dried, in the case of performing a tensile test, has a linear-elastic behavior [GIB99].

The bone material is not defined in the existing database of the ANSYS FEA program that can be directly accessed and used for different types of analyses. As a consequence, in

order to perform the simulation of the experiment, a new type of orthotropic material has been defined, by assigning all the mechanical characteristics of the bone tissue in this case. By considering the hypothetical analysis, as well as the fact that in this case it is aimed to analyze the effect of the mechanical stress in the case of a live organism, in the case of defining the properties of the material there were used the values which are characteristic to a human live tissue (wet) in the end. Table 3.5 presents the characteristic values of the defined material, these values being taken into consideration in the case of the analysis. The values presented in this table are critical for the defined material and are not sufficient to describe the behavior of the analyzed material while testing. In order to describe and completely define the behavior of this material, in the database of the program were introduced the pair of values presented by Gibson [GIB99]. It is important to specify at this stage the fact that the properties of the bone tissue are highly influenced by certain biological factors (age, gender, type of analyzed bone), the values considered and used for the analysis in the case of this research being average values.

Table 3.5. Properties of the compact bone

Characteristic	MU	Value
Density	Kg/m ³	2000
Young's modulus E	GPa	
longitudinal		17
radial		11,5
tangential		11,5
Elastic modulus G	GPa	
longitudinal - radial		3,3
longitudinal - tangential		3,3
radial - tangential		2,3
Poisson's ratio	-	
longitudinal - radial		0,41
longitudinal - tangential		0,41
radial - tangential		0,41
Compression strength	MPa	
longitudinal		193
transversal		133
Tensile strength	MPa	
longitudinal		148
transversal		49

In order to check if the bone material was defined in a correct way, we made a simulation of a collision between the pendulum ball and a medical model which is represented by a piece of skull having the mechanical characteristics and the properties of the new type of material which was defined. Figure 3.40 shows the assembly involved in this simulation, in the initial position before the ball of the pendulum was starting to move. For the boundary condition, the model has been considered in a bounding box, the bounding surface being formed by the patch surface reunion, which delimits the analyzed model. The made analyses had the main aim to theoretically determine the areas in which the fracture of the medical model is expected to occur. As a criterion for estimating the fracture zones, we used the assessment of the main maximum stresses variation (traction and compression stresses) and the comparison of these stresses to the ones given by the fracture stresses given by traction and compression tests in longitudinal direction and transverse directions, as well (see Table 3.5). As it is possible to notice from the variation diagram shown in Fig. 3.41, the main maximum stresses had a value of 380.71 MPa in the case of traction, an 387.62 in the case of compression, these values being above the limit values given for the traction and compression stresses presented in Table 3.5, no matter which type of direction

is considered (longitudinal or transverse). The first conclusion that was drawn was that in the case of a real load, similar with the one that was simulated, it will result at the end for sure the fracture of the analyzed model. In the same time, the analysis of maximum stress area propagation (areas marked in red on the figure) allowed an estimation of the areas where the cracking would occur in the case of a real experiment to be done (Fig. 3.41).

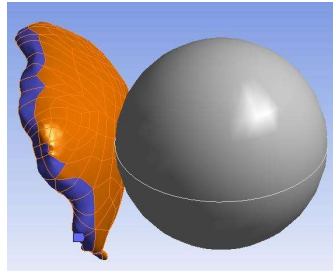


Fig. 3.40. Assembly subjected to impact

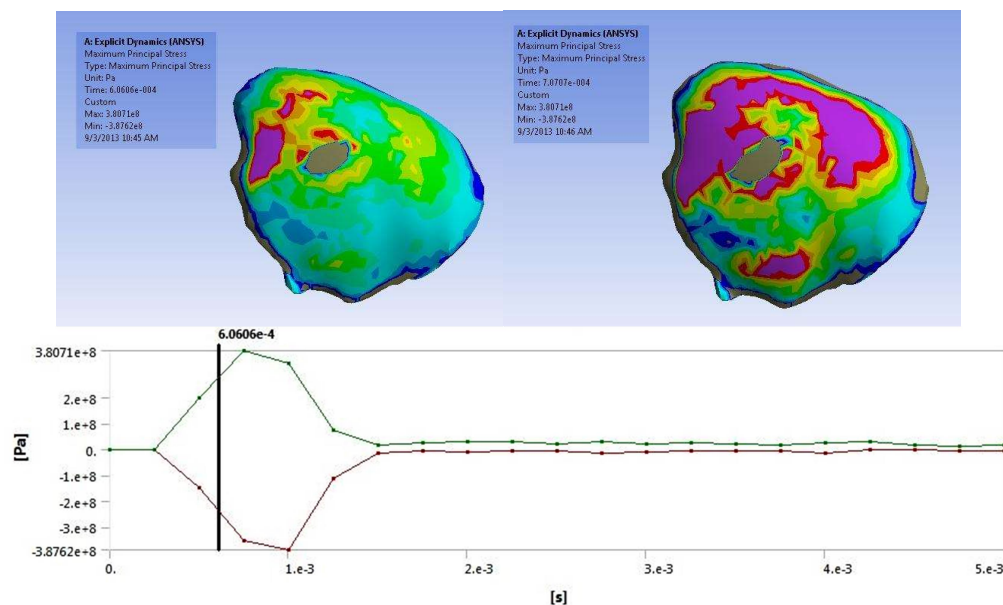


Fig. 3.41. Variation of the maximum principal stress

In order to check the theoretical model presented above, we evaluated a collision between the ball and a skull which was presumed from a body. In order to visualize the striking effects, the experiment was filmed with a high speed camera (8000 frames / second), the analysis made after the experiment allowing to precisely locate the cracks and their

This project has been funded with support from the European Commission. This publication [communication] reflects the views only of the authors, and the Commission cannot be held responsible for any use which may be made of the information contained therein.

propagating directions. After the analysis of the frames filmed during this procedure it was possible to notice that the fracture lines are following the direction of apparent displacement of the zones with maximum stresses, which means that the material that was considered for the virtual analysis has been correctly defined. Materials considered to be used in the case of the implant. The materials used for the manufacturing of the customized implants were polymethylmetacrilate (PMMA) in the shape of a bone cement and titanium alloy TiAl6V4 type, which is delivered in powder state, in order to be processed by selective laser melting, technology which is available at the Rapid Manufacturing laboratory from the Technical University of Cluj-Napoca. The most important mechanical characteristics of the materials used for the fabrication of implants used for the experiments and analyses are presented in Table 3.6. The behavior of these materials for different types of stresses is completely described by stress-strain curves and state equations that are available in the material database of the ANSYS FEA program.

Table 3.6. Properties of the implanted materials

Characteristic	MU	Value	
		PMMA	Ti6Al4V
Density	Kg/m ³	1170 - 1200	4430
Fracture strength (traction)	MPa	38 - 70	950
Yield strength (traction)	MPa	38 - 70	880
Elongation	%	2-10	14
Elasticity modulus E	GPa	2,5 – 3,5	113,8
Poisson's ratio		0,35 – 0,4	0,342
Specific heat	J/kgK	1466	526,3
Thermal conductivity	W/m.K	0,167 – 0,25	6,7

3.4.1. Choosing the type of interaction between models

As previously mentioned, the hypothetic experiment assumes the dynamic analysis of an assembly which consists of three components, to determine the effects that are caused by the dynamical loads induced by the pendulum ball. The source of these effects is the pendulum ball, the effects on the other components being generated by subsequent interactions that occur between the ball and the implant, the implant and the destroyed area and between the assembly and the environment. The definition of these subsequent interactions has a similar importance as the other planned operations of the experiments,

due to the fact that in this case, through this operation will be defined the way how the stresses will be transmitted within the experiment. The order in which these interactions are defined can be freely established by the user, the only conditions being to adequately define these interactions in accordance with a possible real experiment. A first interaction consists in the interaction between the assembly and the environment, and mainly between the boundary conditions of the assembly, which must be realized in such a way that the model will be statically defined during the entire experiment. In this sense, the surface elements which limits the destroyed area (Fig. 3.42) are considered as being locked (a constraint that does not allow any degree of freedom and which generates within the fixed element reactions that are oriented along all three directions O_x , O_y and O_z of the reference frame). The surface elements on which the boundary condition is applied are manually selected by the user.

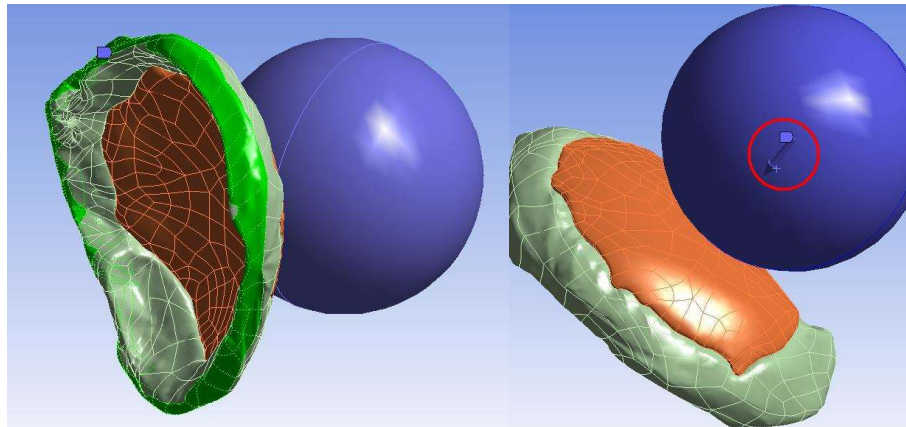


Fig. 3.42. Clamping of surface elements

Fig. 3.43. Impact between the sphere and the implant

The interaction that stressed the assembly was given by the collision of the pendulum ball against the implant (Fig. 3.43). The value of the ball velocity was determined by the energy conservation law (4.47 m/s), its direction being considered for the most disadvantageous situation, along a direction which is perpendicular to the surface of the implant, in such a way that there will not be any tangential components to produce a decrease of the impact energy and by consequence an attenuation of the striking effects. With the aim of maintaining the impact energy at a constant level it was considered that the contact between the ball and the implant is realized with no friction. The most important

This project has been funded with support from the European Commission. This publication [communication] reflects the views only of the authors, and the Commission cannot be held responsible for any use which may be made of the information contained therein.

interaction was between the implant and the destroyed area, due to the fact that through this contact region the stresses from the implant to the surrounded life area are transmitted. The definition of this interaction was limited to the definition of the contact type which exists between the surface elements that exist at the boundary, on the implant and on the destroyed area, as well. Due to the shape errors that occur during the CAD generating process, the contact between the implant and the destroyed area was not realized on the entire boundary, but just on a certain number of surface elements. There were considered as being in contact those surface elements, with a zero distance between them and a tolerance of 10–6 mm. This means that it is obligatory that after the decimal point, the first five significant numbers will be zero, otherwise it can be considered that the surfaces are not in contact.

As it was previously presented, from the practical point of view, dimensional deviations of 1 mm do not have a significant influence on the functionality of the implant. By taking into consideration the geometrical shape of the patched surfaces, a manual selection of those which are in contact was practically impossible, the best option being the automatic selection (Fig. 3.44) as it was done with the finite element analysis program, the type of the contact being defined at the end by the user.

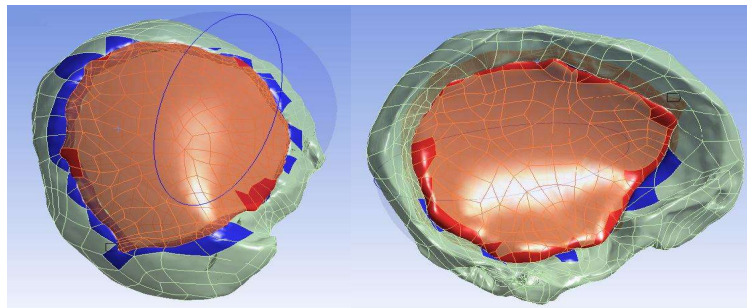


Fig. 3.44. Surface elements of the implant and destroyed area being in contact

From the type of contacts which are possible to be used within the dynamical explicit analyses, such as the presented one, just two were adequate and recommended to be used in this case. The first type was the bounded type contact, which presumes the assumption by the finite element analysis program of different internal conditions which does not allow the displacement of the components during the simulation, which at a superficial analysis seems to correspond to the contact conditions that are required to be imposed in this case for such a type of analysis. With all these specifications set, during the simulations that were made

with the aim of planning the experiments, it was possible to notice that the implant is being displaced from the destroyed area that is considered as reference, without producing any mechanical stress in this area (Fig. 3.45). Such a behavior is generated by the fact that, due to the shape error, during the stress period it is allowed the deformation of the implant, leading to a final effect that consists in the separation of the components and their simultaneous displacement.

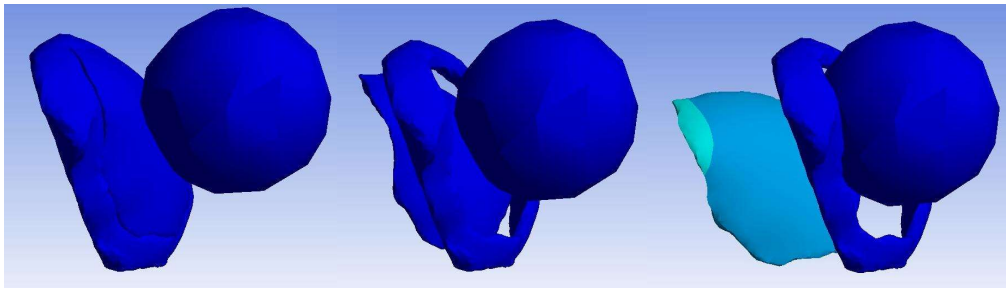


Fig. 3.45. "Bonded" contact type

The problem related to the displacement of the components while stressing has been solved by imposing a contact with friction between the components. The following equation is already well known:

$$F_f = \mu \cdot N \quad (3.4)$$

where: F_f is the friction force, μ – friction coefficient, and N – normal force on the surface on which the friction acts.

If in this relationship, the friction coefficient is considered as having a unit value ($\mu = 1$), i.e. the friction force which acts on any surface becomes equal to the normal force on that surface, which means in this case there is an integral transfer of the forces to the surface area of interest.

So as that the stresses generated by the impact between the ball and the implant will be transferred as adequate as possible, the value of the friction coefficient μ between the implant and the destroyed area has been imposed at 0.99, this value being the maximum value which is allowed by the program.

The previous experiment shown in Fig. 3.45 was repeated in similar conditions, the only difference consisting in the way the contact between the two components is realized. Figure 3.46 shows the results obtained in the case of the new experiment that was made, the

differences compared to the previous experiment that was analyzed being clearly visible. The ball representation was removed from this figure for a better view and to ease the evaluation of the results.

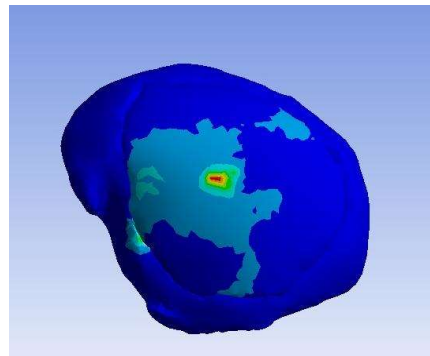


Fig. 3.46 Frictional contact

3.4.2. Determination of the experiment period

The simulation period is influenced by the time required for the development of the interaction between the pendulum ball and the assembly formed by the implant and the destroyed area, value that has been loaded as input element in the program in which the simulation is realized. In the following the time of the interaction will be named as the period of the experiment, period which is influenced by the initial relative positions between the ball and the assembly formed by the implant and the destroyed area, this period representing the time while the ball of the pendulum is in motion. In order to determine the optimum periods for the experiments, we made simulations by keeping the geometrical shapes of the models involved, models that comprise simplified hypotheses that were imposed in this sense. The materials that were tested were the generic ones, their behavior being defined as purely elastic (materials with zero plasticity and which do not present residual deformations after the stressing), without being introduced a common value of the fracture stress. The value of the fracture stress (a mechanical characteristic that is mandatory to be used for defining the behavior of a material) that has been considered for the analysis had two higher size orders as compared to the one of the materials involved in the real simulation (the fracture stress of the generic material was approximately 100 times

higher as compared to the one of the real material). By taking into consideration the simplified hypotheses that were considered it is possible to state that in the case of testing experiment, the pendulum ball is moving along the incident direction until its total energy becomes equal with the potential energy of elastic deformation that it is stored in the impacted assembly, the ball being rejected at this time period, its displacement being continued in the opposite direction, this moment being the one in which the analyzed assembly is considered as being stressed with a maximum force. The appreciation of the moment in which the two energies are equal was realized by analyzing the stress diagrams that resulted at the end of the testing experiments (Fig. 3.47).

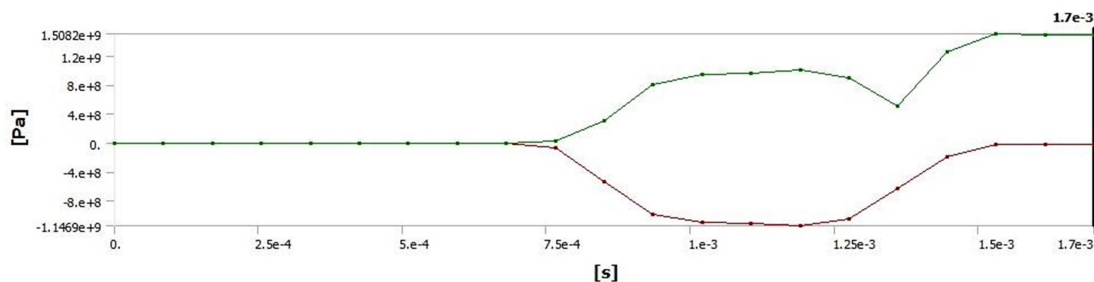


Fig. 3.47. Justifying diagram used for selecting the duration of the experiment

As one may notice in Fig. 3.47, the value of stresses that are stored in the analyzed assembly presented an increasing tendency until a critical value was reached, followed by a decrease of the stresses, which correspond to the overlapping of the moment in which the values of the two energies are equal, when the ball already changed the direction of its motion. In order to determine the optimum period of the experiment there we made simulations with different time periods that were varied between 0.5 ms and 2.5 ms (the precise values were: 0,5; 0,7; 1; 1,2; 1,5; 1,7; 2; 2,5 ms). By analyzing the stress diagrams corresponding to these testing experiments it was possible to notice that the two resulted energies were equal at 1.2 – 1.3 ms time period. The optimum value of the experiment period was 1.7 ms, this value being considered a covering period that allowed the rejected ball to be displaced to the initial position and to get out from contact with the analyzed assembly. Figure 3.47 shows only one of the analyzed cases, this analysis being realized with respect to the aspects that were presented above and justifying meantime the selected choice. The realization of the experiment tests with variable periods was required to fulfil

the initial objective, allowing on the one hand the realization of the analysis without the time limitation of the interaction period, and on the other hand, allowing the possibility to determine simulation time periods as lower as possible at the end. During the experiments, the time required for performing the simulation varied from 6 hours for a 0.5ms time period of interaction to 28 hours for 1.7 ms time period and 48 hours for 2.5 ms time period, the differences being in all these cases, as one may notice, significant in the end. It can be specified the fact that the period of the experiment which was selected is specific to the designed experiment, being influenced by the relative position that has been imposed between the ball and the assembly that formed by the implant and the destroyed area considered in the analysis. For any other relative position of the models involved in the experiment, the time period selection for the experiment assumes the repetition of the experiment tests and the re-interpretation of the stress diagrams obtained in this way after the analysis.

3.4.3. Results

The virtual analysis of a hypothetical impact between the customized implant and a tough body was realized for 4 distinctive cases, by considering different shapes of the customized implants (solid and compact implants and perforated) and different types of materials for the manufactured implants made by SLS and SLM (PMMA in the bone cement state and TiAl6V4 powder alloy material). The assemblies implant- destroyed area realized in this way, were impacted by a pendulum in a similar way with the situations previously described. Figure 3.48 illustrates the schematic representation of these simulations in the initial position.

The effects of the dynamic stress were evaluated in close connection with the stresses stored in the implant and those transferred by the implant to the destroyed area due to the fact that from the stressing point of view, there is a comparison term given by the fracture strength (at traction and compression) of the analyzed material. The analysis of the strains generated by the dynamic stress is purely informative.

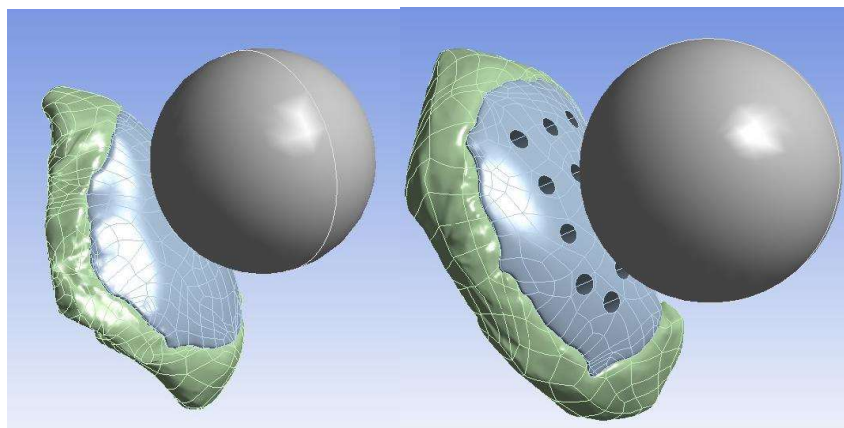


Fig. 3.48. Assemblies considered for the analysis

The size of the strains is difficult to be evaluated due to the fact that the results that are obtained are expressed in percents and the determination of the effective size of the deformations raise difficult problems due to the irregular shape of the analyzed models and their non-uniform thickness as well. As evaluating criteria for the determination of the stresses there were considered the von Mises equivalent stress and the maximum main stresses, the realized analysis being similar with the one realized for the validation of the material models.

The stress distribution in the case of the 4th analysis case is presented in the following images, for the assembly implant- destroyed area and for the destroyed area, as well.

1. Implant with solid structure made from PMMA (Fig. 3.49 and Fig. 3.50)

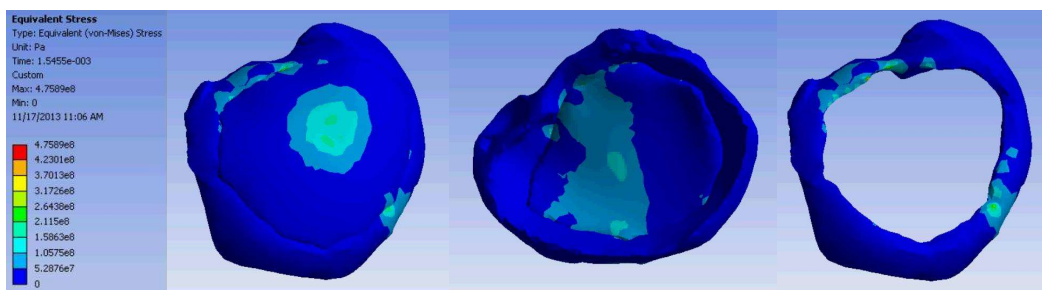


Fig. 3.49 Equivalent stress

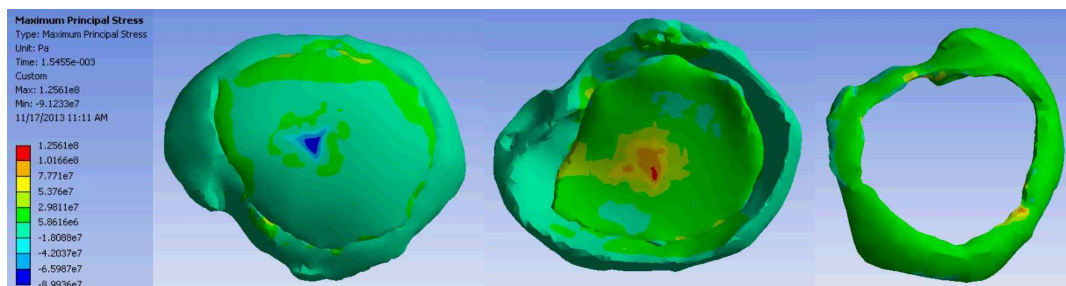


Fig. 3.50. Maximum principal stress

2. Perforated implant made from PMMA (Fig. 3.51 and Fig. 3.52)

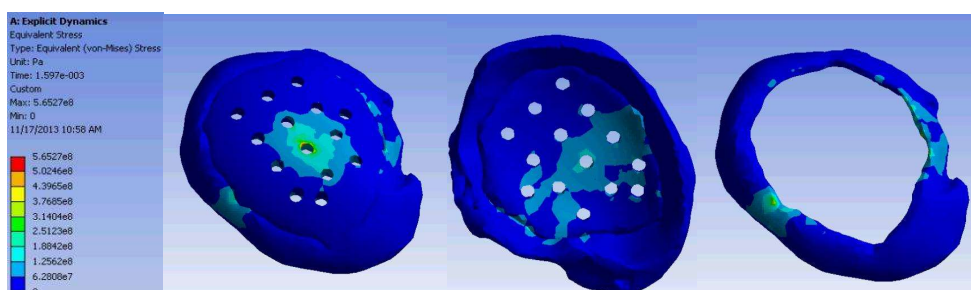


Fig. 3.51. Equivalent stress

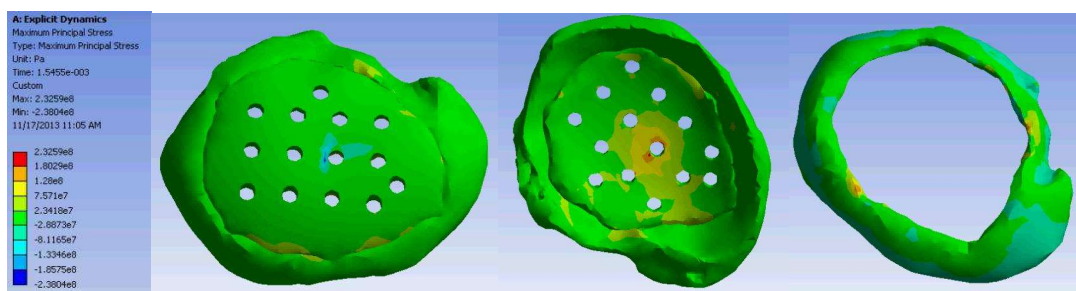


Fig. 3.52. Maximum principal stress

3. Implant with solid structure made from TiAl6V4 (Fig. 3.53 and Fig. 3.54)

This project has been funded with support from the European Commission. This publication [communication] reflects the views only of the authors, and the Commission cannot be held responsible for any use which may be made of the information contained therein.

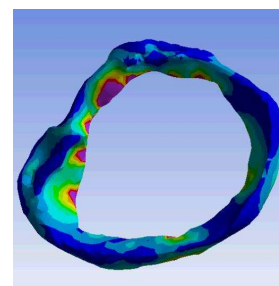
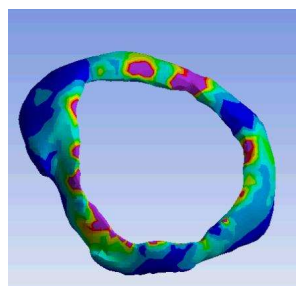
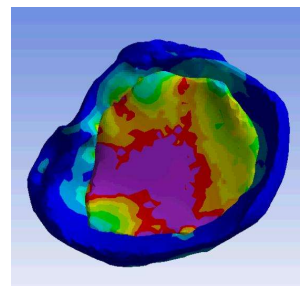
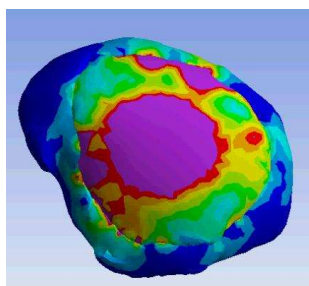
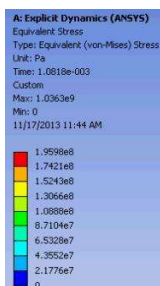


Fig. 3.53. Equivalent stress

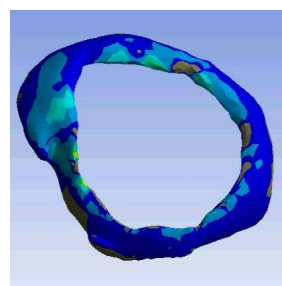
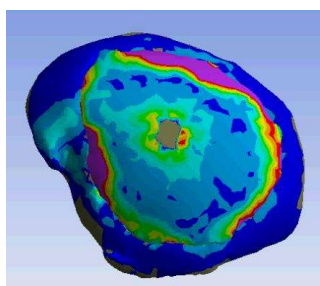
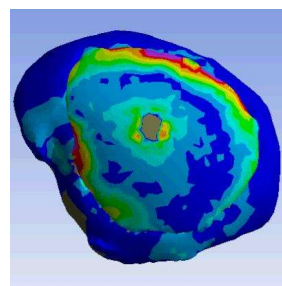
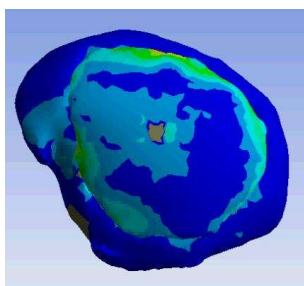


Fig. 3.54. Maximum principal stress

4. Perforated implant made from Ti6Al4V (Fig. 3.55 and Fig. 3.56)

This project has been funded with support from the European Commission. This publication [communication] reflects the views only of the authors, and the Commission cannot be held responsible for any use which may be made of the information contained therein.

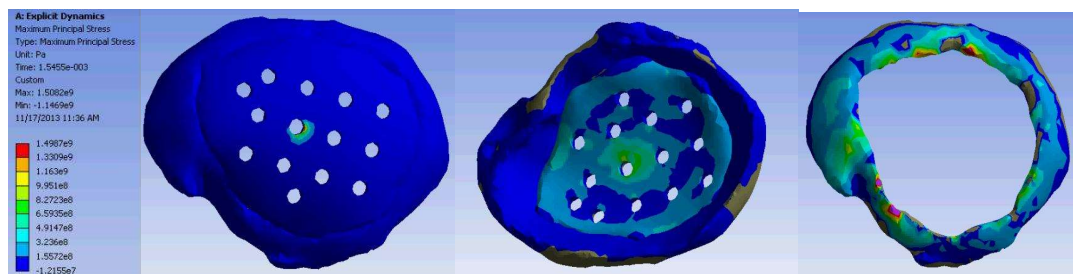


Fig. 3.55. Equivalent stress

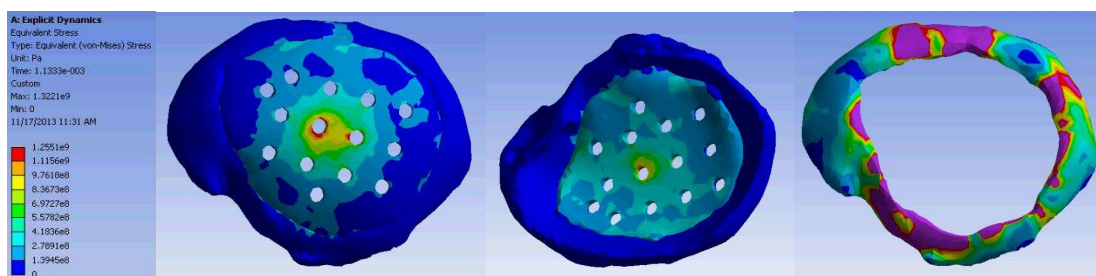


Fig. 3.56. Maximum principal stress

By taking into consideration the conditions in which the impact simulation was realized it was considered that in all cases the general stress of the assembly generated by the ball of the pendulum is identical, the value of the stresses stored in the components of the assembly only depending on the properties of the materials from which these components are made from. Table 3.7 lists the value of these stresses sorted out by considering the analyzed component and the experiment which was simulated.

Table 3.7. Stress values

	PMMA		Ti6Al4V	
	Implant	Destroyed area	Implant	Destroyed area
Solid	$\sigma_{echiv} = 475 \text{ MPa}$	$\sigma_{echiv} = 435 \text{ MPa}$	$\sigma_{echiv} = 195 \text{ MPa}$	$\sigma_{echiv} = 509 \text{ MPa}$
	$\sigma_{min} = -89,9 \text{ MPa}$	$\sigma_{min} = -46,8 \text{ MPa}$	$\sigma_{min} = -77 \text{ MPa}$	$\sigma_{min} = -79 \text{ MPa}$
	$\sigma_{max} = 125 \text{ MPa}$	$\sigma_{max} = 103 \text{ MPa}$	$\sigma_{max} = 109 \text{ MPa}$	$\sigma_{max} = 195 \text{ MPa}$
Perforated	$\sigma_{echiv} = 565 \text{ MPa}$	$\sigma_{echiv} = 408 \text{ MPa}$	$\sigma_{echiv} = 125,5 \text{ MPa}$	$\sigma_{echiv} = 470 \text{ MPa}$
	$\sigma_{min} = -238 \text{ MPa}$	$\sigma_{min} = -38 \text{ MPa}$	$\sigma_{min} = -120 \text{ MPa}$	$\sigma_{min} = -39,5 \text{ MPa}$
	$\sigma_{max} = 232 \text{ MPa}$	$\sigma_{max} = 98 \text{ MPa}$	$\sigma_{max} = 149,8 \text{ MPa}$	$\sigma_{max} = 412 \text{ MPa}$

The virtual simulations that were made had the main objective to determine the optimum geometrical shape of the customized implants and the adequate materials from which these implants should be made, in such a manner that the realized implants would exhibit a maximum safety for the patient to be operated at the end. In the simulating processes, as material to be used in the case of the implant, there were considered two types of materials with mechanical characteristics that are completely different. These types of materials were polymethylmetacrilate (PMMA) in the bone cement state and TiAl6V4 alloy in the powder state. As regarding the shape and structure of the implant, there were considered for the analyses two cases: one in which the implant has been considered in compact state (with a fully solid structure) and other in which the implant presents perforations. The presence of the perforations can be medically justified, these perforations blocking the accumulation of liquid between the implant and the soft surrounding tissues, this liquid if present generating an unwanted pressure on these types of structures.

After the analyses and after the interpretation of the results it was possible to draw some important conclusions, such as:

- The stress state of the assembly components is strongly influenced by the type of material from which the implant is manufactured. In this sense, the implants made from PMMA material stores stresses that are much higher as compared to the case when the implants are made from metallic materials, the Young's modulus that has lower values in the case of plastic material leading to a decrease of the stress transferred to the surrounding structures as compared to the case when the implant is made from metallic materials.
- The decrease of the implant stiffness by realizing some perforations leads to an increase of the stress state of the implant simultaneous with a decrease of the stress level that is transmitted to the surrounding structures, without being influenced by the state of the material from which the implant it is made with.
- The weight of the implant made from PMMA is three times lower as compared to the weight of the implant made from titanium alloy material.
- By considering the thermal properties (specific heat and thermal conductivity) of the two types of materials considered for the analyses it was possible to notice that the implants made from PMMA material have isolating properties superior as compared to the ones of the metallic material, leading to the patient increased comfort in the end.

This project has been funded with support from the European Commission. This publication [communication] reflects the views only of the authors, and the Commission cannot be held responsible for any use which may be made of the information contained therein.

Figure 3.57 shows the medical implant that was manufactured at the Technical University of Cluj-Napoca of PMMA material by using 3D printing and Rapid Tooling methods (Selective Laser Sintering and Vacuum casting). The implant made of PMMA material (as illustrated in Fig. 3.57) presents perforations. The presence of the perforations can be medically justified, these perforations blocking the accumulation of liquid between the implant and the soft surrounding tissues, this liquid if present generating an unwanted pressure on these types of structures.

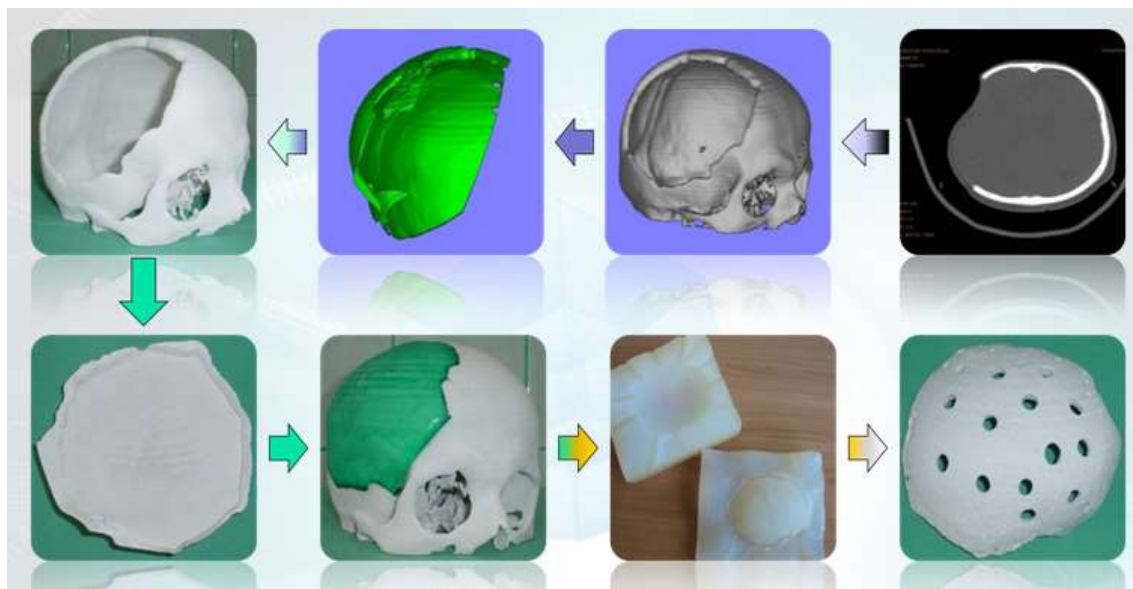


Fig. 3.57. Manufacturing of medical implant by SLS and Vacuum casting

3.5. Finite element analysis to determine the mechanical characteristics of cervical discs

In this study six cervical cages have been designed as an alternative to cervical discs. Solid Works software was used for the design. These new proposed implants have two or four "ears" with the role to fix the cage on neighboring vertebrae, with the role of preventing migration after implantation. The implant can be fixed with the help of self-tapping screws, from Ti alloys. The 3D models for the proposed implants are presetted in figures 3.58-3.63.

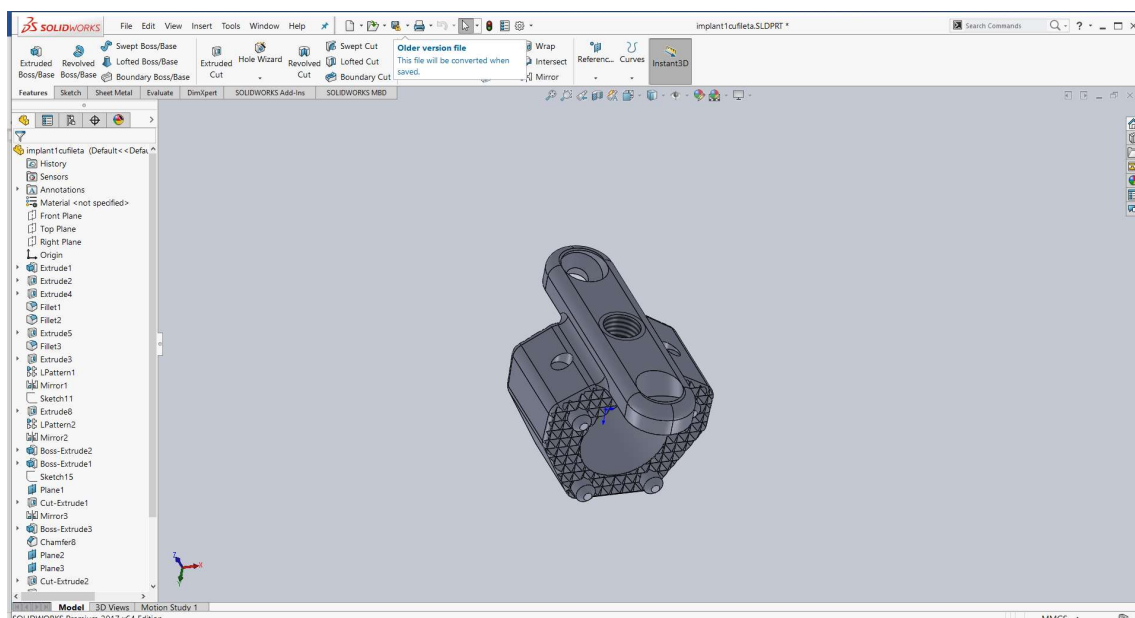


Fig. 3.58. 3D model for the first implant

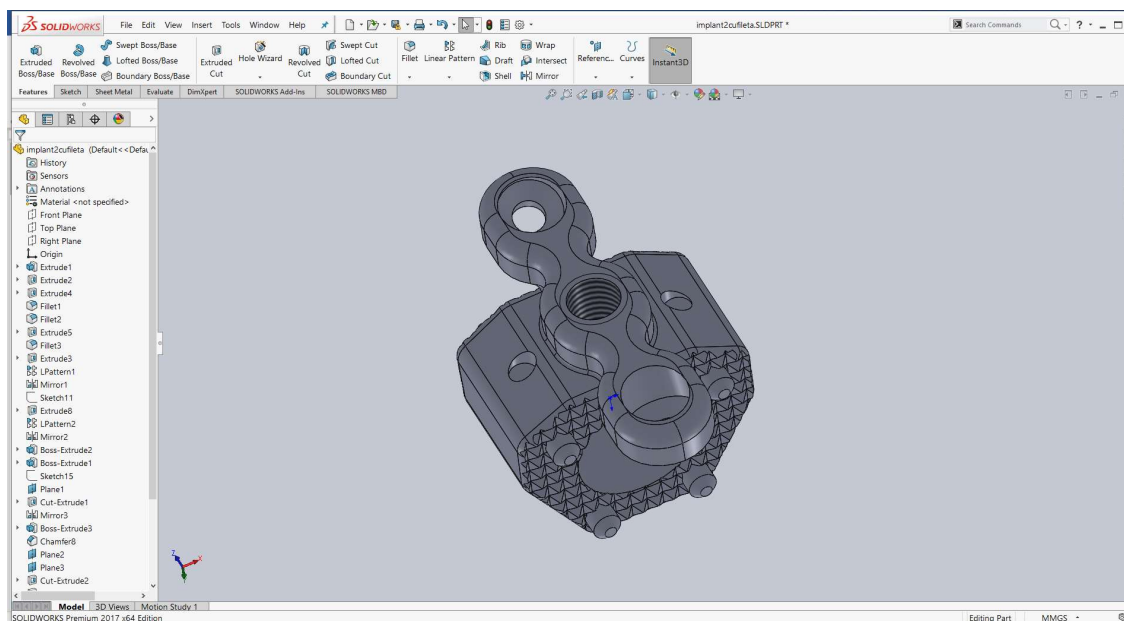


Fig. 3.59. 3D model for the second implant

This project has been funded with support from the European Commission. This publication [communication] reflects the views only of the authors, and the Commission cannot be held responsible for any use which may be made of the information contained therein.

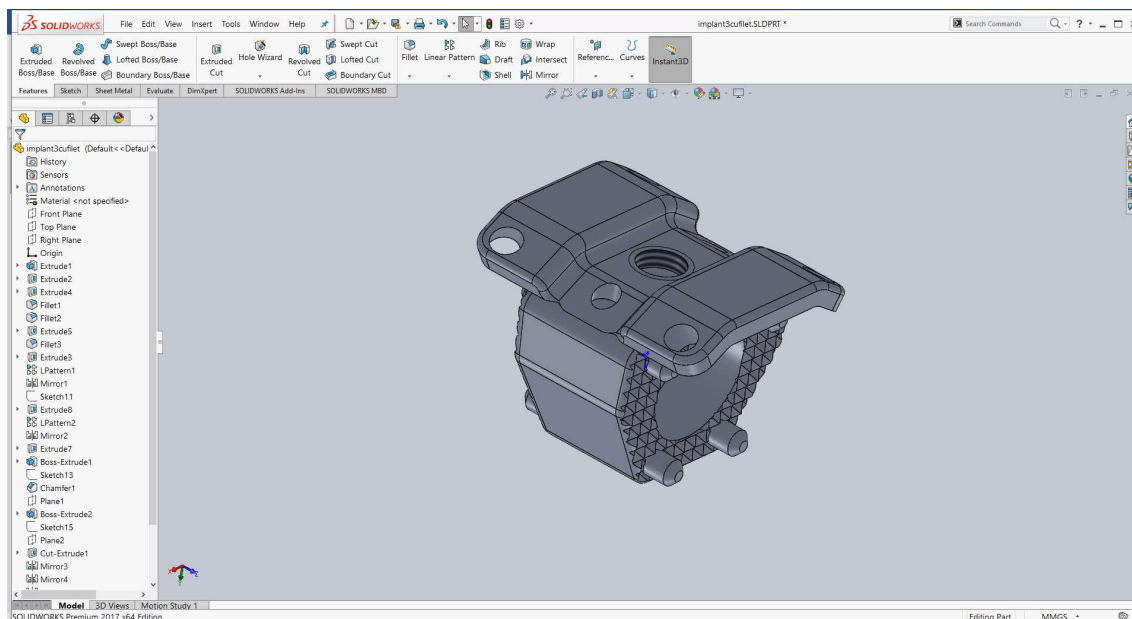


Fig. 3.60. 3D model for the third implant

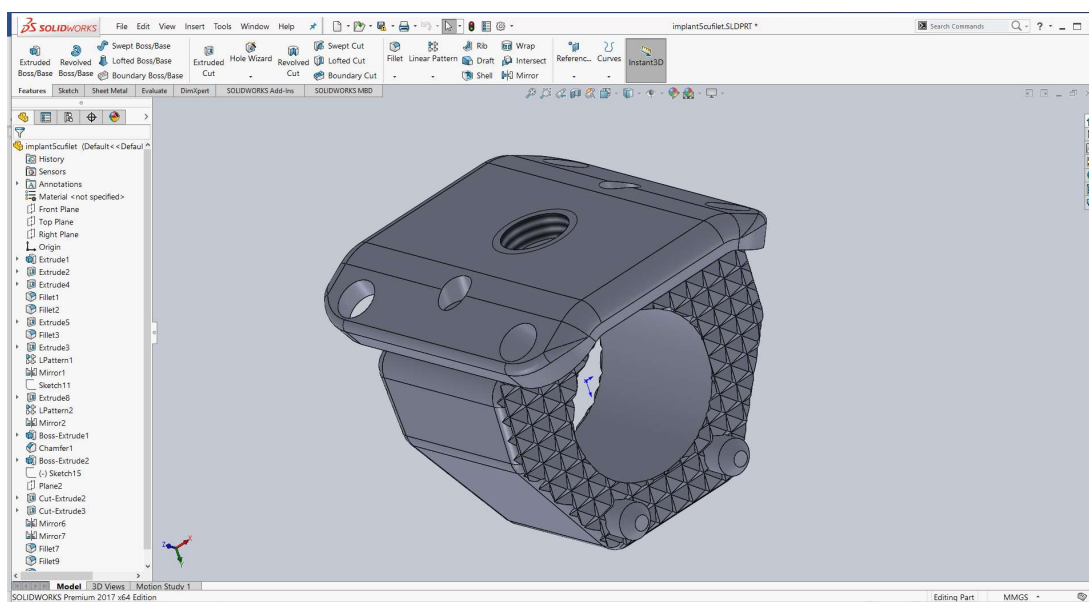


Fig. 3.61. 3D model for the fourth implant

This project has been funded with support from the European Commission. This publication [communication] reflects the views only of the authors, and the Commission cannot be held responsible for any use which may be made of the information contained therein.

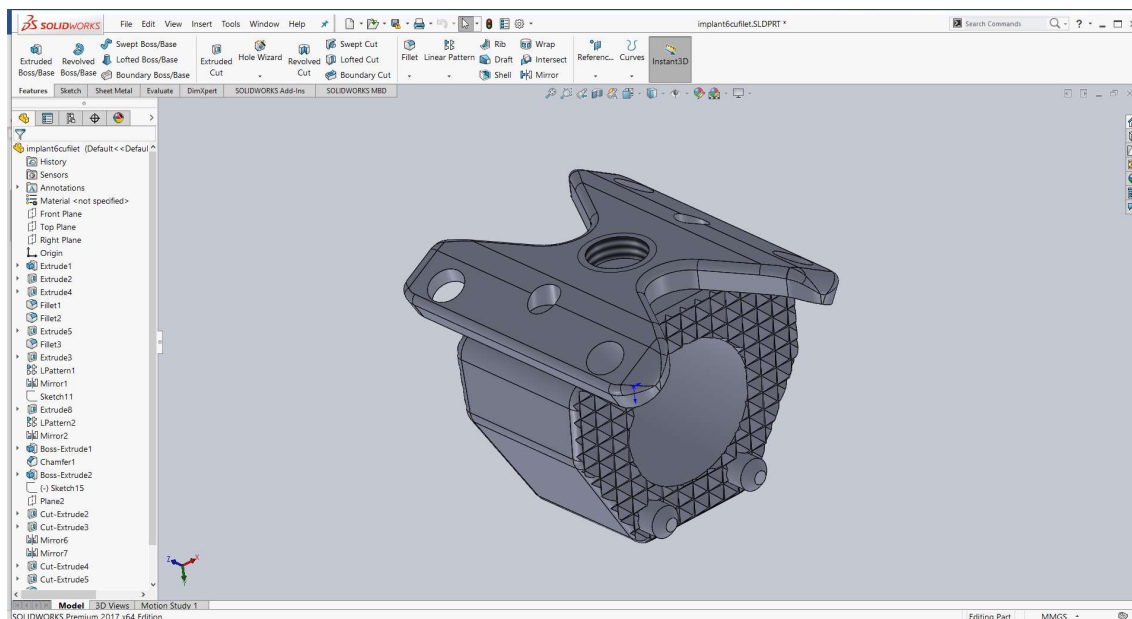


Fig. 3.62. 3D model for the fifth implant

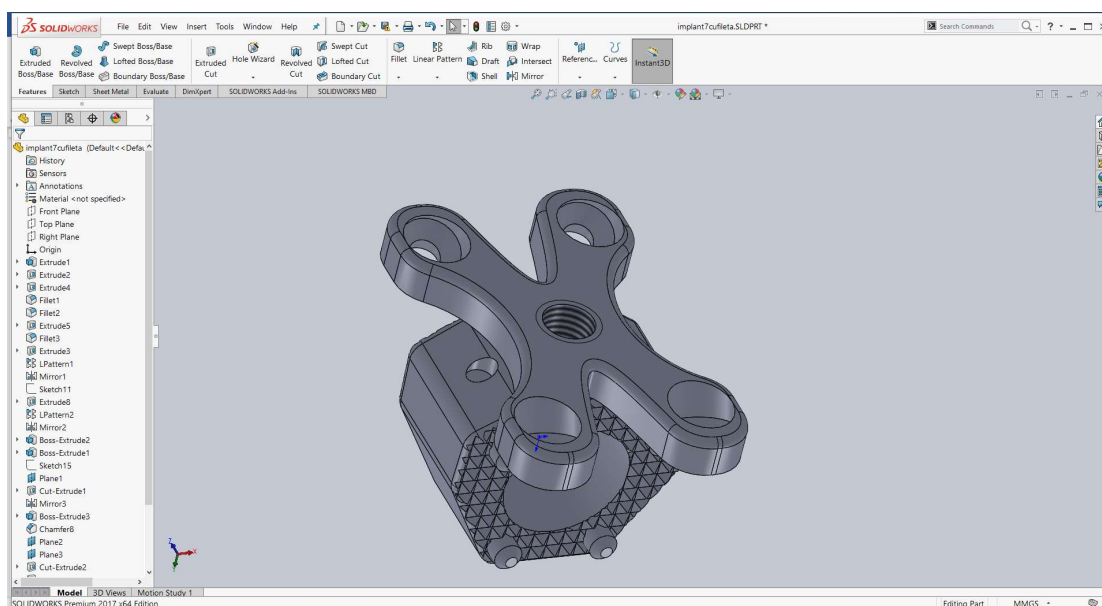


Fig. 3.63. 3D model for the sixth implant

This project has been funded with support from the European Commission. This publication [communication] reflects the views only of the authors, and the Commission cannot be held responsible for any use which may be made of the information contained therein.

With the help of the finite element method, the characteristics of an implant used to replace the cervical intervertebral disc, can be analyzed and improved in order to prevent its migration, to facilitate the surgery and to evaluate his behavior during extension of the head. For this reasons flexural and extension test were applied for the 3D models.

Numerous studies have been performed in the field of cervical spine stress, that can be found in the specialized literature. The weight on the spine increases dramatically when the head is bent forward at varying degrees. In a neutral position the head of an adult weighs 10 to 12 pounds. The forces applied to the neck when the head tilts forward surges to 27 pounds at 15 degrees, 40 pounds at 30 degrees, 49 pounds at 45 degrees and 60 pounds at 60 degrees. The model prediction at 90 degrees neck position was not reliable. Taking into account the flexion of the head for the analysis of the forces in the cervical spine, the pounds were transformed into kilograms and after in Newtons (Table 3.8).

Table 3.8. Forces applied to the cervical spine at different angles of the neck

Position	Neutral	15	30	45	60
Force applied to the Cervical Column [N]	45-54	122	181	222	271

As a theoretical situation, when the bending force and the extension force are equal, it is considered a variant. In order to analyze the force and stress in the fixed area of the implant, a Finite Element Analysis was performed using ANSYS 16.0. The finite element model was loaded in compression and flexion cases for all six cervical disc models analyzed, for both used implant materials. Pure Ti and PEEK were analysed in the case of maximum load (271 N). These materials can be used in the Cage manufacturing.

The mechanical properties of PEEK parts manufactured by SLS are: density 1310 kg/m³, tensile modulus 4250 MPa, tensile strength 90 MPa, strain at break 2.8% [WWW07] and for pure Ti, manufactured at 120 W on SLM, the mechanical properties are: density 4510 kg/m³, tensile strength 440 MPa, Young's modulus 100 GPa, Poisson's ratio 0.35 [ISP2016, MIR17]. The mechanical properties for PEEK were token from the Material Data Sheet (EOS GmbH - Electro Optical Systems, EOS PEEK HP3) [WWW07] and for pure Ti from previous research in scientific literature [ISP2016].

The proposed goal was to analyze and determine the stress state, the compression and the deformation of the implants. For discretization of the implants (mesh size of 0.5 mm) were used finite elements. The mesh details are presented in Table 3.9.

Table 3.9. Mesh details from FEA of the implants

Details of "Mesh"	
Display	
Display Style	Body Color
Defaults	
Physics Preference	Mechanical
<input type="checkbox"/> Relevance	0
Sizing	
Use Advanced Size Func...	Off
Relevance Center	Coarse
<input type="checkbox"/> Element Size	Default
Initial Size Seed	Active Assembly
Smoothing	Medium
Transition	Fast
Span Angle Center	Coarse
Minimum Edge Length	6,4903e-003 mm
Inflation	
<input type="checkbox"/> Patch Conforming Options	
<input type="checkbox"/> Patch Independent Options	
Advanced	
<input type="checkbox"/> Defeaturing	
Statistics	
<input type="checkbox"/> Nodes	51758
<input type="checkbox"/> Elements	30164
Mesh Metric	None

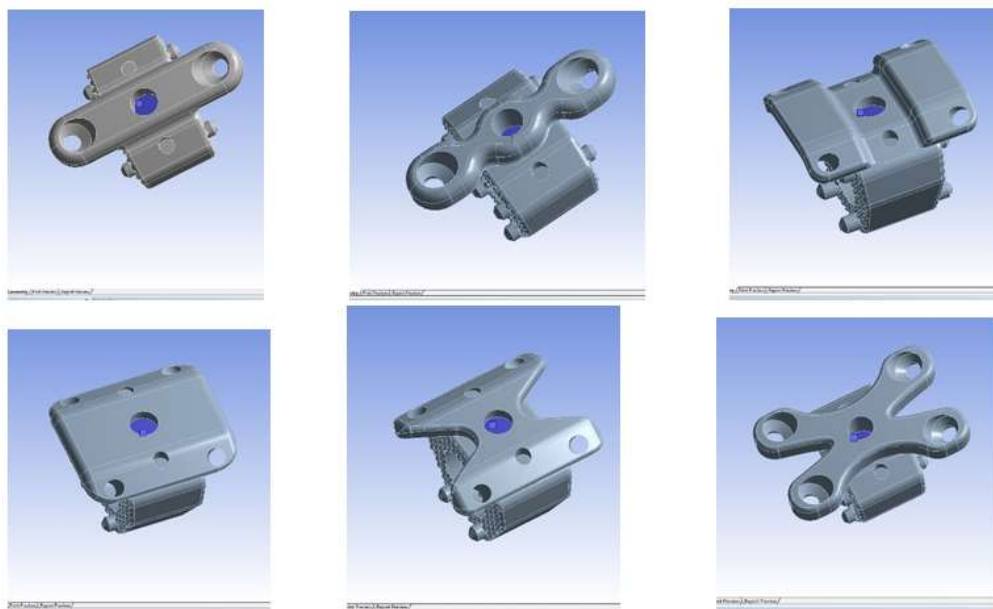


Fig. 3.64. Boundary conditions applied to each implant

This project has been funded with support from the European Commission. This publication [communication] reflects the views only of the authors, and the Commission cannot be held responsible for any use which may be made of the information contained therein.

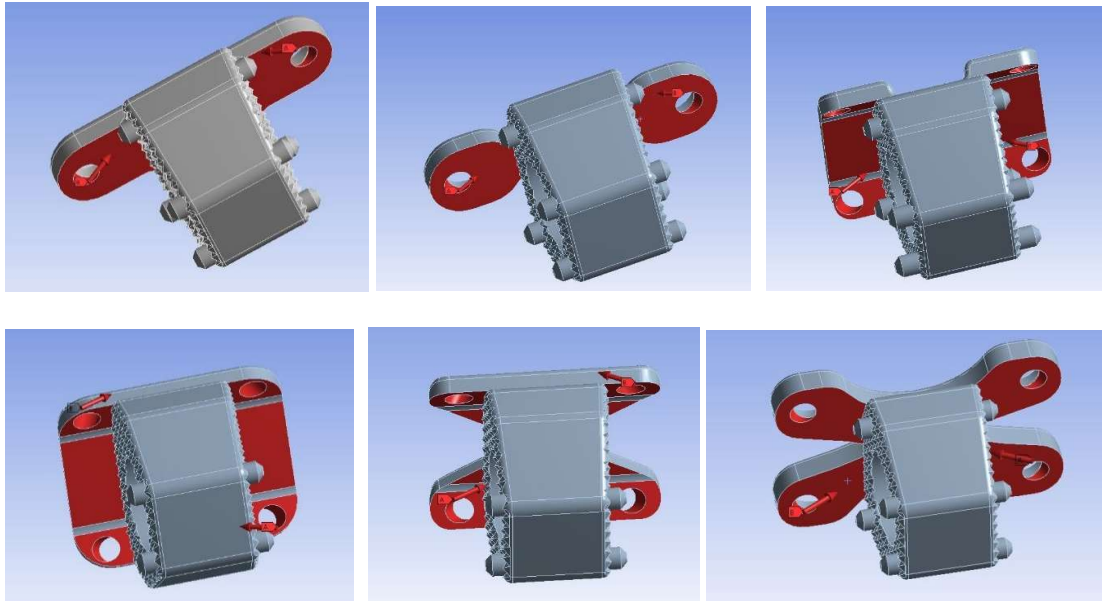


Fig 3.65. External loads applied to each implant

The proposed implants with two "ears" for fixing the cage on neighboring vertebrae were loaded by forces acting on the right and left sides of the implant (the contact areas with screws). It was considered that the force value of 271 N should be evenly distributed on both sides of the part, so the left side and the right side individually carried a force of 135.5 N (traction).

Figures 3.66 and 3.67 show the distribution of the von Mises stress in the implants for pure Ti and PEEK materials, respectively. For the proposed implants with four "ears" for fixing the cage on neighboring vertebrae (Figure 3.66(c)-(f) and Figure 3.67(c)-(f)) the forces are applied on the contact area with the screws. Every screw hole from the left side and the right side of the part carries a force of 67.75 N (traction), considering that the total force of 271 N is equally distributed to the set of four screw holes. A comparative study was made between both used materials, PEEK and Ti, for the distribution of the von Mises stress (see Figure 3.68). It can be observed that the difference between these two materials of the maximum von Mises stresses values is very small. The lowest difference was observed in the case of implant no 3 (0.051 MPa) and the highest was for implant no 6 (1.625 MPa). Thus, these two used materials have a good behavior from the point of view of stress tests.

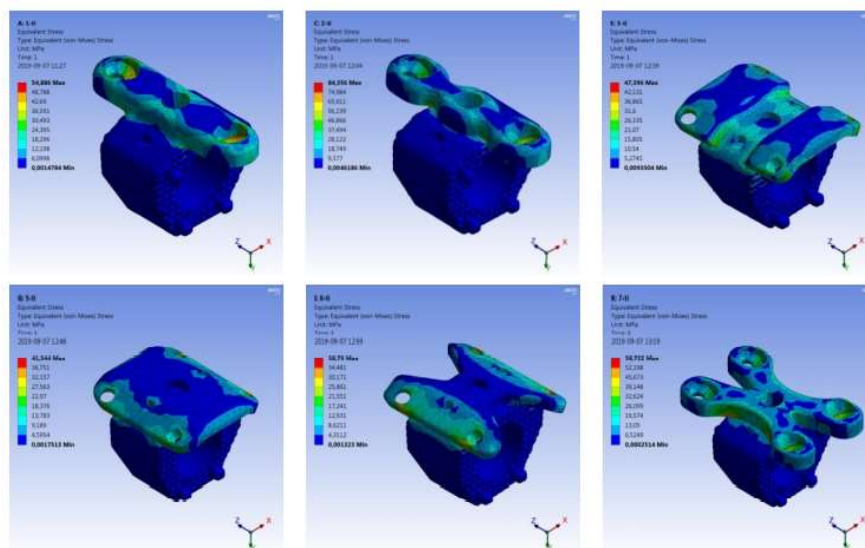


Fig. 3.66. Distribution of the von Mises stress for pure Ti material: a- implant model no 1; b- implant model no 2; c- implant model no 3; d- implant model no 4; e- implant model no 5; f- implant model no 6.

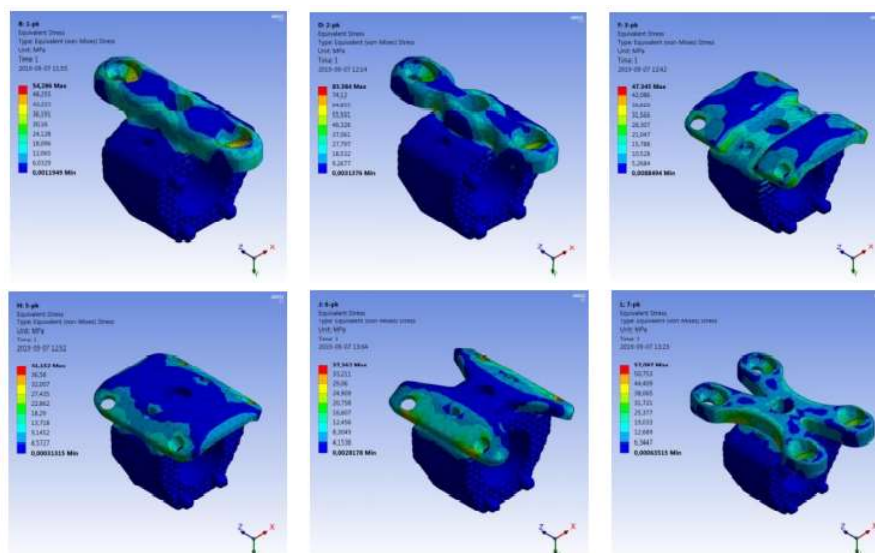


Fig. 3.67. Distribution of the von Mises stress for PEEK material: a- implant model no 1; b- implant model no 2; c- implant model no 3; d- implant model no 4; e- implant model no 5; f- implant model no 6.

This project has been funded with support from the European Commission. This publication [communication] reflects the views only of the authors, and the Commission cannot be held responsible for any use which may be made of the information contained therein.

Table 3.10. Values of the von Mises equivalent stress obtained by FEA

	The von Mises stress distribution at traction for the six cervical implants [MPa](a.-f.)					
	a.	b.	c.	d.	e.	f.
Pure Ti	54.886	84.356	47.396	41.344	38.79	58.722
PEEK	54.286	83.384	47.345	41.152	37.362	57.097
	The von Mises stress distribution at compression for the six cervical implants (a.-f.)					
	a.	b.	c.	d.	e.	f.
Pure Ti	55.074	222.19	57.576	19.914	41.702	63.156
PEEK	54.564	118.29	53.202	19.767	41.741	63.222

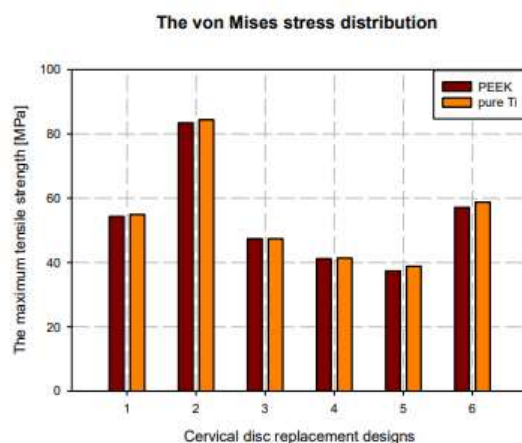


Fig. 3.68. Comparison between the values of the von Mises equivalent stress for all six implants

Table 3.11. Total deformations obtained by FEA

	Total deformation for the cervical implants (a.-f.) loaded in traction [mm]					
	a.	b.	c.	d.	e.	f.
Pure Ti	0.001908	0.002751	0.002161	0.001264	0.001567	0.006253
PEEK	0.048979	0.070514	0.054247	0.03149	0.039257	0.15664
	Total deformation for the cervical implants (a.-f.) loaded in compression [mm]					
	a.	b.	c.	d.	e.	f.
Pure Ti	0.006666	0.026674	0.006607	0.00252	0.004493	0.014882
PEEK	0.16564	0.31616	0.16153	0.061454	0.11126	0.36764

This project has been funded with support from the European Commission. This publication [communication] reflects the views only of the authors, and the Commission cannot be held responsible for any use which may be made of the information contained therein.

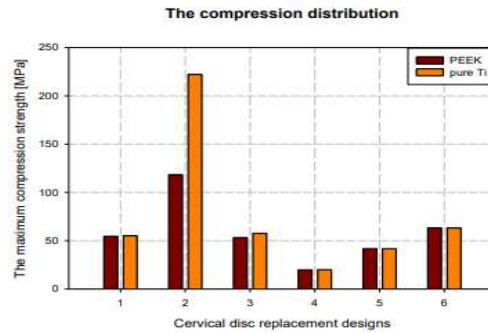


Fig. 3.69. Comparison between the displacement values for all six implants

The analysis proposed to determine the stress state during extension of the head and the deformation of the implant. The total force of 271 N was considered uniformly distributed on both sides of the implant. The part with two holes was loaded by a force of 135.5 N (in traction or compression), while the part with four holes was loaded by a force of 67.75 N (in traction or compression). In the traction tests, it could be observed that the difference between the maximum von Mises stress values of these two materials was very small, lower than 1 MPa for the first four implant models and lower for implants no 5 and 6. The highest difference was found for model no 6 (1.625 MPa). Thus, from the point of view of stress distribution for the traction tests, these two materials have a good behavior for all six implant models. In the compression tests, it was observed that the difference between the maximum von Mises stress values of these two materials was also very small (lower than 1 MPa), only in the case of model no 3 it was 4.372 MPa, and the highest difference (103.9 MPa) was found for the implant model no 2. From the point of view of the compression tests, these two used materials have a good behavior, excepting the implant model no 2. The deformation in case of traction or compression is higher for the PEEK material than in the case of pure Ti material. The PEEK material has a higher elasticity than the Ti material that is more rigid, suggesting that the PEEK material is more suitable for these applications.



Fig. 3.70. Cervical disc implants manufactured by SLM (before the supports were removed)

4. Finite element analyses for medical applications using ABAQUS

4.1. Structural analysis of a bone fixator

4.1.1. General introduction about basics and use of ABAQUS FEA program for medical applications

ABAQUS is a well-known, high quality finite element analysis software, intended for solving the Multiphysics related problems. As such, it is also suitable for medical applications, and there are many examples of its use in the field of biomedical engineering.

Generally, the steps in performing structural analysis of medical products are the same as the steps needed to perform structural analysis of any product. Those are problem definition, preprocessing, processing, postprocessing and report creation. The second, third and fourth step are typically performed in FEA software, and include: import of a geometrical model, removal of unnecessary details and geometry simplification, model reduction based on symmetry, material characterization, definition of loads and boundary conditions, mesh creation, and analysis and review of the results. Creation and transformation of a CAD model, although not performed in FEA software, are also important parts of preparation of a FE model for medical analysis.

Some of the steps in structural analysis of medical products are very specific. Namely, creating a suitable CAD model and defining material properties of biological tissues and organs (such as a bone tissue and bone), which are situated inside the human body, are difficult tasks that must rely on medical imaging [PET18] and reverse engineering techniques [VUL11], [KOR10], [VIT13].

Here we focus on the use of ABAQUS in biomechanics, namely in structural analysis of human bone-joint system coupled with bone fixators. Bone fixators, internal or external, are medical devices used in treatment of bone fractures. Through the following example, all previously mentioned steps in FEA will be illustrated.

4.1.2. Use of ABAQUS in structural analysis of a bone fixator

Internal fixation represents a well-established approach for treating long bone fractures, especially in the proximal femur. Similar to other fixation devices, the selfdynamisable internal fixator (SIF) represents the ultimate standard in internal fixation

This project has been funded with support from the European Commission. This publication [communication] reflects the views only of the authors, and the Commission cannot be held responsible for any use which may be made of the information contained therein.

(Fig 4.1). SIF is a medical device characterized by a modular structure, extensively used by Mitkovic et al. [MIT12], [MIC10]. In clinical studies, they observed that screw breaking occurred in 2.6% of the fixations and that the bar broke at the connection to the trochanteric unit in 0.3% cases [MIT12]. The recorded percentage of SIF failures was small, but it also showed that there was room for improvement in SIF durability [KOR19a]. For this purpose, FEA was employed, and performed in ABAQUS [KOR15]. For a known fixator configuration and position relative to the bone (Fig. 4.2), structural analysis was used to assess bone and fixator deformations, stresses, and strains, which can be related to the fixator durability and the success of bone healing.

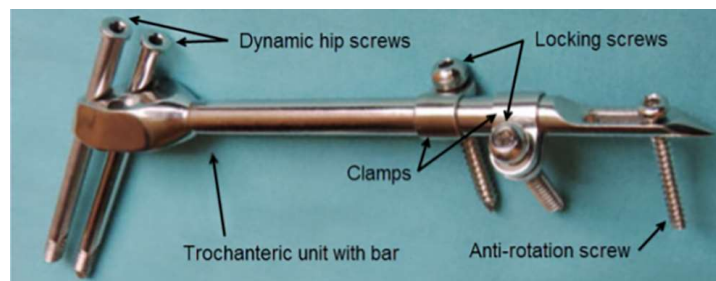


Fig. 4.1. Components of a selfdynamisable internal fixator (SIF) configured for subtrochanteric femoral fracture treatment [KOR19b].

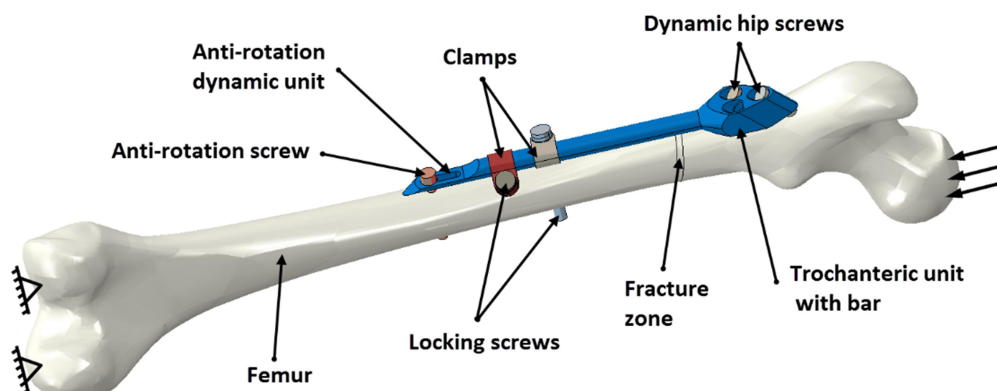


Fig. 4.2. Assembly containing CAD models of femur and SIF [KOR19b].

4.1.3. Creating the CAD model of femur based on CT images

The process of creating subject specific model of human femur was performed through the following stages [KOR10]:

1. Creating the polygonal model of the femur
 - a. Acquisition of CT image set
 - b. Separation of regions of interest (ROIs)
 - c. Creating the point cloud based on CT image set
 - d. Creating the polygonal model based on the point cloud
2. Creating the CAD model of the femur
 - a. “Cleaning” and “healing” of the polygonal model
 - b. Creating a closed group of NURBS surfaces
 - c. Creating a volume model based on surfaces

4.1.3.1. Creating the polygonal model of the femur

The polygonal model is obtained by creating a network of triangular surfaces based on the point cloud, which is primarily intended for visualization of data and their transfer to the CAD software package. After “cleaning”, this model can be used for other purposes, such as creating surface and solid models of bones [KOR10], [VUL11], or producing physical models by additive manufacturing technologies [STO09], [MIL09].

In this research, a computational tomography (CT) image set (tomogram) of the lower extremities of a patient was used as a starting point for making the CAD and FEM models of the femur. A CT image set represents a series of two-dimensional X-ray images created in parallel planes (Fig. 4.3).

Using a computer application for medical images processing, a separate ROI was selected on the tomogram of the lower extremities, which contained the femur of the patient's right leg. Using the function for recognizing the tissue type based on density, a point cloud corresponding to the outer surface of the femur and the surface separating the compact bone from the central medullary cavity was created.

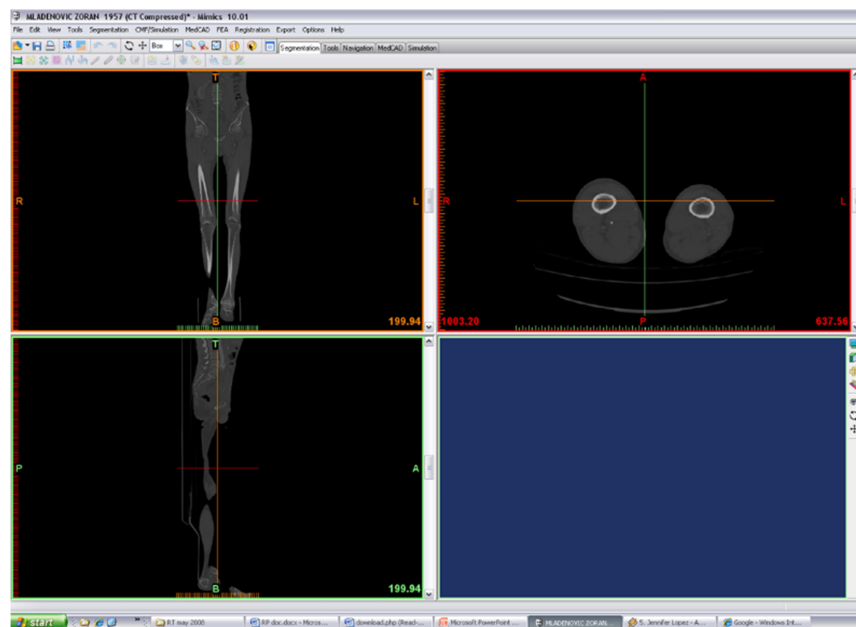


Fig. 4.3. Patient-specific CT image set of lower extremities [KOR10]

The tomogram originated from a patient who had problems with the vascular system. So called „contrast material” was injected into his veins during the scan, the density of which was similar to the density of bone. Therefore, the isolated point cloud also contained a part of the vascular system, as can be seen in the picture of the polygonal model obtained based on it (Fig. 4.4).



Fig. 4.4. Polygonal model of the femur created from point cloud that had been extracted from CT image set [KOR10]

This project has been funded with support from the European Commission. This publication [communication] reflects the views only of the authors, and the Commission cannot be held responsible for any use which may be made of the information contained therein.

4.1.3.2. Creating the CAD model of the femur

Processing of the polygonal model that served as a basis for creating the CAD model of the femur, begun with the removal of segments that obviously did not belong to the femur, such as parts of the vascular system or parts of surrounding bones (Fig. 4.5).



Fig. 4.5. Polygonal model of the femur, after removal of unnecessary objects [KOR10]

After removing the excessive polygons, the next step was "cleaning" the inside of the model and removing the "noise" that originated mainly from the internal trabecular structure of the bone (Fig. 4.6). All mentioned operations were performed in CATIA.



Fig. 4.6. The internal structure of the polygonal model of the femur before cleaning [KOR10]

After removing the inside, the remaining outer surface of the bone was still connected to the segments that penetrated deeper into the inside (Fig. 4.7) and contained cracks and openings that needed to be filled (Fig. 4.8).

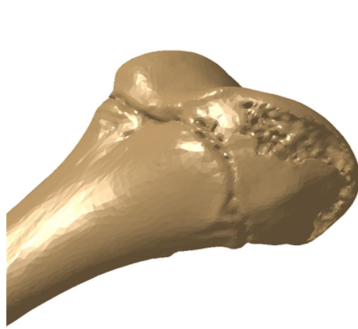


Fig. 4.7. In the polygonal model, zones consisting of "chaotically" arranged triangles were present, which were the consequence of osteoporotic changes in the bone [KOR10]

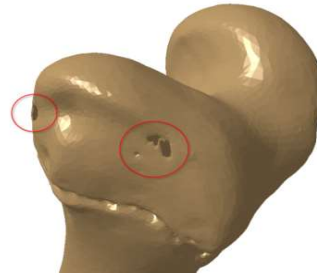


Fig. 4.8. The holes on the surface of the polygonal model were most often connected with larger groups of irregularly spaced polygons that penetrate deep into the interior of the model [KOR10]

After the polygonal model was satisfactorily healed and its surface smoothed, a closed NURBS surface was created by approximation of polygonal model, which represented the outer shell of the model (Fig. 4.9). Based on this surface, a volume model of the femur was created using a simple procedure.

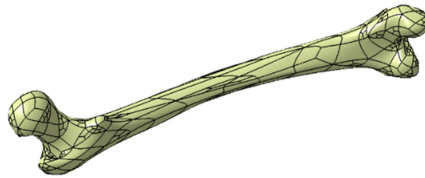


Fig. 4.9. Surface model obtained from the polygonal model [KOR10]

4.1.4. Meshing and defining of the material characteristics

4.1.4.1. Defining material characteristics

The first phase in creating a FE model of the femur is defining material characteristics. In bone modeling, two approaches are generally used:

1. Zoning of bone CAD model interior, i.e., its division into segments which are then assigned equivalent material characteristics.

2. Assigning material characteristics to each finite element individually, by correlations with the density of the material, which, in turn, is determined on the basis of CT image sets,

The first approach involves the creation of zones that correspond to the internal structure of the femur. In addition to the zones that are clearly separated, compact bone and central medullary cavity, the rest of the internal volume, which is filled with spongy bone, may also be divided into several zones (Fig. 4.10). The idea behind the process is relatively simple, but it has a number of drawbacks. The major one is the use of average elastic properties that are assigned to different bone segments, as elastic properties of bone tissue may vary significantly throughout the bone volume. This is especially true for long bones like femur or tibia. Recognition and creation of zones inside the bone also requires significant time and effort, which does not speak in favor of this option, especially concerning subject - specific FEA.



Fig. 4.10. Zones created inside the solid model of the femur, which are later used in meshing process (approach 2). Zones are created to approximately represent the segments of different trabecular bone density. The zone representing cortical bone is omitted for clarity [KOR10]

The second approach, local material mapping, implies the assignment of unique elastic properties to each finite element of the bone model, based on the density of bone tissue at the corresponding location, which is obtained from CT images. Empirical equations are used to establish relations between reported CT image grey values and tissue density, as well as between tissue density and elastic properties [SCH08, HEL08]. As commercial FEA codes often accept only a limited number of material definitions (material cards), the whole range of possible values of an elastic property, like Young's modulus, is usually subdivided into a number of intervals, and each finite element is assigned a mid-value of the interval to

which its calculated value belongs. This approach is often used in practice because it allows the FE model to be created in a very short time and accounts for local variation of bond density. However, errors still can be made in representing the interior of the bone, especially if the dimensions of the finite elements are significantly larger than the thickness of the individual bone segments.

Details on advantages and drawbacks of each approach may be found in [KOR13]. In this research, the second approach, local material mapping, was used to create the finite element (FE) model of bone-fixator assembly. Nevertheless, both approaches had alternatively been applied throughout authors' practice to create FE model of femur, as described next.

4.1.4.2. Approach 1 to assigning material characteristics to femur – used for comparison with approach 2

Separate zones inside the model were created, representing cortical bone and medullary cavity [KOR13]. The volume of spongy bone was divided into several zones, according to the usual distribution of trabecular density (Fig. 4.10). Material characterization was performed by assignment of constant Young's modules to the elements belonging to cortical bone zone and to the elements belonging to spongy bone zones. A very small value of Young's modulus (1 MPa) was also assigned to elements inside medullary cavity, where bone marrow is situated. Material properties ($E_{\text{cortical}}=12.7$ GPa, $E_{\text{trabecular}}=0.07-0.3$ GPa) were defined using trial and error approach, in order for the model to have the same value of maximum displacement as the model created using approach 2. The model was meshed using average edge size of 3 mm at the bone surface and fast element growth towards the inside of the bone (Fig. 4.11). Details on FE model may be found in Table 4.1.

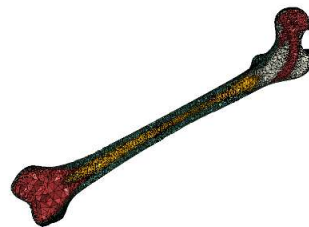


Fig. 4.11. Cross-section of zoned femur FE model with constant averaged properties
[KOR10]

Table 4.1. Material characterization, model sizes and maximal values of displacement, stress and strain field variables for various FEM models of the same subject – specific femur.

Femur model	Material characterization	Number of elements	Number of nodes
1	Zoned, $E_{cortical}=12.7\text{GPa}$, $E_{trabecular}=0.07$ and 0.3GPa	149 712	217 726
2a	Mapped, 20 material definitions	59 926	98 298
2b	Mapped, 100 material definitions	59 926	98 298
2c	Mapped, 300 material definitions	59 926	98 298

4.1.4.3. Approach 2 to assigning material characteristics to femur – used in current research

Only the external femur surface was reconstructed from CT images. Femur volume was meshed with quadratic tetrahedron elements, with average edge size of 3 mm at the bone surface and fast element growth towards the inside of the bone defined (Fig. 4.12) [KOR13]. Material mapping was performed in order to assign material properties to all elements, using the empirically obtained relation between HU values and bone density (Eq. 4.1) and relation between bone density and Young's modulus taken from [MOR03] (Eq. 4.2). Three variations of the model were created, (model 2a, model 2b and model 2c), using 20, 100 and 300 discrete values of Young's modulus, covering the range from 0 to 19GPa. Details on FE model may be found in Table 4.1.

$$\rho_{app}[g/cm^3] = 0.1957 + 0.001053 HU \quad (4.1)$$

$$E[N/mm^2] = 6950 \cdot \rho_{app}^{1.49} \quad (4.2)$$

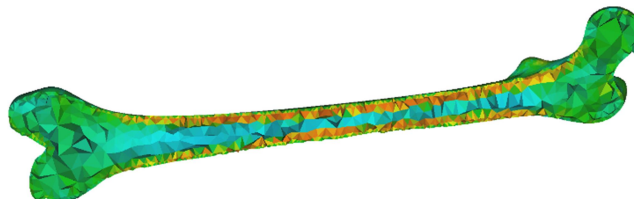


Fig. 4.12. Cross-section of femur FE model, with mapped material properties [KOR13]

This project has been funded with support from the European Commission. This publication [communication] reflects the views only of the authors, and the Commission cannot be held responsible for any use which may be made of the information contained therein.

4.1.5. Creating FE model of femur-fixator assembly

The FEM model of femur-fixator assembly was created through the following steps:

1. Creation of parametric CAD model of fixator in CATIA using standard form features.
2. Assembly of CAD models, with parametrical positioning.
3. Creation of screw holes by subtraction of fixator model from femur model in CATIA.
4. Surface partitioning on femur CAD model, to create surfaces for loads and supports definition.
5. Import of CAD model into ABAQUS.
6. Creation of fracture zone on femur using split techniques in ABAQUS.
7. Assignment of material properties to fixator and fracture zone, and temporary material properties to the rest of the femur.
8. Definition of contact properties and contacts between assembly components.
9. Definition of loads and supports.
10. Meshing of all components.
11. Export of meshed femur FE model from ABAQUS.
12. Import of meshed femur FE model into medical imaging software and material mapping, based on grey values from CT images.
13. Duplication of created assembly in ABAQUS.
14. Import of femur FE model with mapped material properties into ABAQUS and replacement of femur FE model in duplicated assembly with mapped FE model.
15. Redefinition of contacts, where necessary.

CAD model of SIF (Fig. 4.13) was created in CATIA using standard solid modelling form features that may be found in all modern CAD software, like extruded or revolved protrusions or cuts, rounds or chamfers. Length of trochanteric bar, as well as clamps and screws linear positions and angles were parametrized, to enable each possible standard configuration of SIF to be created. Standard configurations of SIF are mutually different by bar length. During a surgery, clamps and screws are positioned in different ways, depending on femoral shape and fracture position. CAD model of SIF, i.e. SIF subassembly, was assembled with solid model of the femur that had been created earlier (Fig. 4.2). Holes in femur were created in assembly model, by subtracting SIF geometry from femur geometry.

Two surface partitions were created on femur surface (Fig. 4.16). The first surface partition was created on femoral head, in order to represent the contact with acetabulum.

This was the surface on which the load was later applied. The second surface partition was created on femoral condyles, to represent the knee. This was the surface on which the support was later added. CAD model of the SIF-femur assembly was imported into ABAQUS. Two parallel planes were then created near upper trochanter. The femur was cut with the planes and a new volume was created inside the femur to represent a simple subtrochanteric fracture (Fig. 4.16).

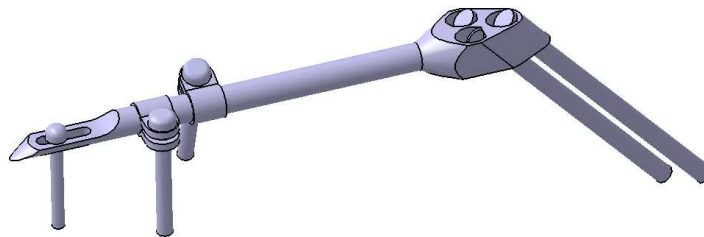


Fig. 4.13. CAD model of SIF, with bar length equal to 150 mm.

The elasticity of fracture zone was set directly in ABAQUS, taking one of the three fixed values corresponding to three different stages of fracture healing process. Elasticity modulus of 1160N was used to simulate the elasticity of fracture zone 3 weeks after the surgery, while modules of 2055 N and 4220 N were used to simulate the elasticity after 6 and 12 weeks respectively. As experimental data were not available, the values were predicted by multiplication of rat femur related data reported in [KOM05] by ratio of typical values of cortical bone elasticity modules for human and rat femur. SIF material, stainless steel (ASTM F 138-2) was modeled using elasticity modulus of 2.1 GPA. Yield strength of SIF components equals to 795 N/mm^2 [OLD12], while yield strength of cortical bone, which mainly supports the screws, is reported to fall between 104 and 120 N/mm^2 [KOR53], [BUR76], [VIN85]. Coefficient of friction was set to 0.34 between the bone and SIF components [MIS02] and to 0.7 between SIF components.

Temporary material properties (arbitrary elasticity modulus and Poisson's ratio) were at first assigned to femur, in order for the initial FE model to be created and meshed. After meshing, the FEM model of the femur was exported and imported into a medical imaging program, where material mapping was performed, as described earlier. Hundred incremental values of elasticity modulus were used in the study, ranging from 1 N/mm^2 to 17500 N/mm^2 (Fig. 4.14).

This project has been funded with support from the European Commission. This publication [communication] reflects the views only of the authors, and the Commission cannot be held responsible for any use which may be made of the information contained therein.

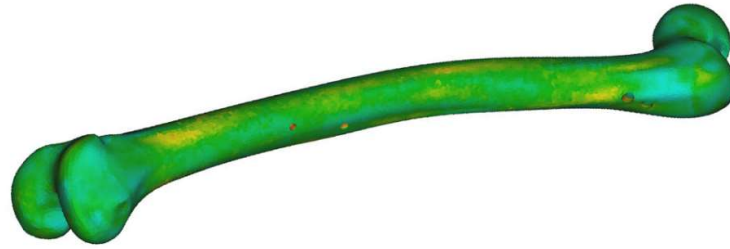


Fig. 4.14. FE model of femur with assigned material properties. Screw holes are visible on the model [KOR15]

After material mapping was performed, the FE mesh was exported from medical imaging software and imported back to FEA software as so called “orphan mesh” (elements only, no geometry), where it was reassembled with SIF in a duplicate assembly model. Contacts that were lost after femur replacement were recreated. The FEM model of the whole femur-SIF assembly, with created mesh, is shown in Fig. 4.15. Element colors are shown by material properties, that is why SIF and fracture zone elements have same colors and femur elements come in many colors (hundred different colors, as hundred discrete material cards were used during material mapping).

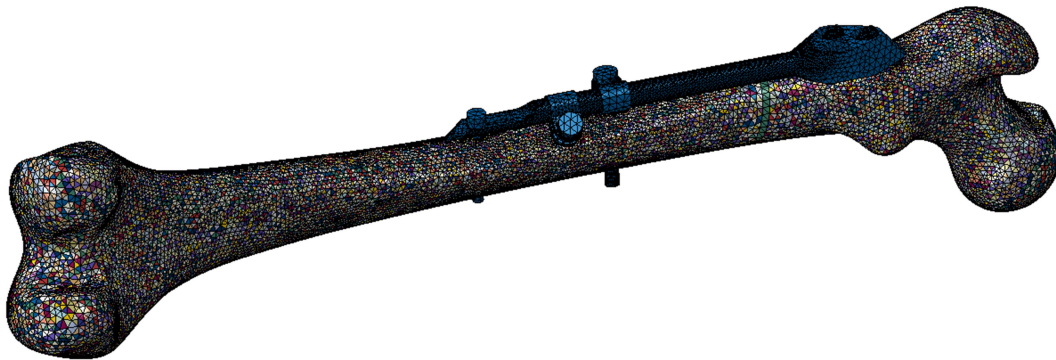


Fig. 4.15. Finite element model of femur-SIF assembly, including fracture zone.

4.1.6. Loads and boundary conditions

Loading conditions were set to roughly resemble the one-legged stance. The movement of nodes belonging to a surface created on the distal femur, similar to the area

This project has been funded with support from the European Commission. This publication [communication] reflects the views only of the authors, and the Commission cannot be held responsible for any use which may be made of the information contained therein.

that comes in touch with meniscus, was fixed in all directions. Distributed load of 883 N (equivalent to body weight of 90 kg) was set to act on a surface created on femur head, that would come in touch with acetabulum (Fig. 4.16).

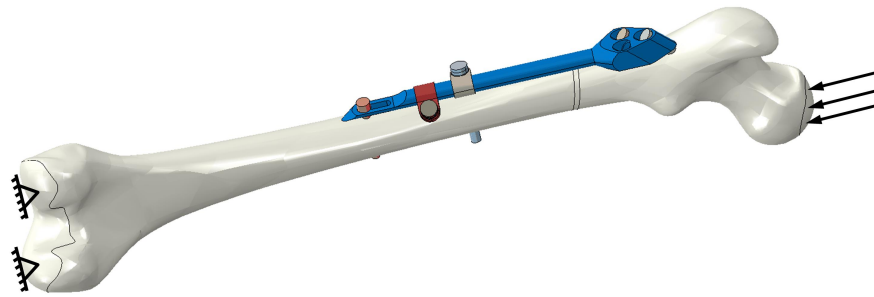


Fig. 4.16. Schematic representation of loading conditions imposed on FE model [KOR15]

4.1.7. Analysis results

Typical equivalent stress distribution, which was obtained by analysis of various FE model instances defined within the study, is shown in Fig. 4.17. From stress distribution it is obvious that the bar and hip screws are dominantly loaded in bending. The highest stress was localized on upper part of hip screws and around one of the screw holes in trochanteric unit. The calculated stresses in femur were the highest around screw holes, but they were in no case larger than 29.58 N/mm². For the presented load case, the worst values of safety factor were found to be 3.51 on femur and 6.58 on SIF (on distally further hip screw).

4.1.8. Conclusions

Finite element models of bones and bone-joint system, used to predict and prevent bone fractures or loosening of bone-implant assemblies, have proven to be a very useful tool in biomechanics. The work of numerous researchers is contributing to their noticeable advance in the last decade, especially in defining material models of bone tissue.

The presented procedure for creating a FE model of the femur based on a CT image can, with minor modifications, be used to model any bone or bone system in the human body and simulate the behavior of bones and bone - implant systems under various external

loads. It has been used by authors to perform various studies, including a study of SIF sensitivity to number bar length, number of screws and elasticity of fracture zone that depends on the number of weeks after the surgery [KOR15].

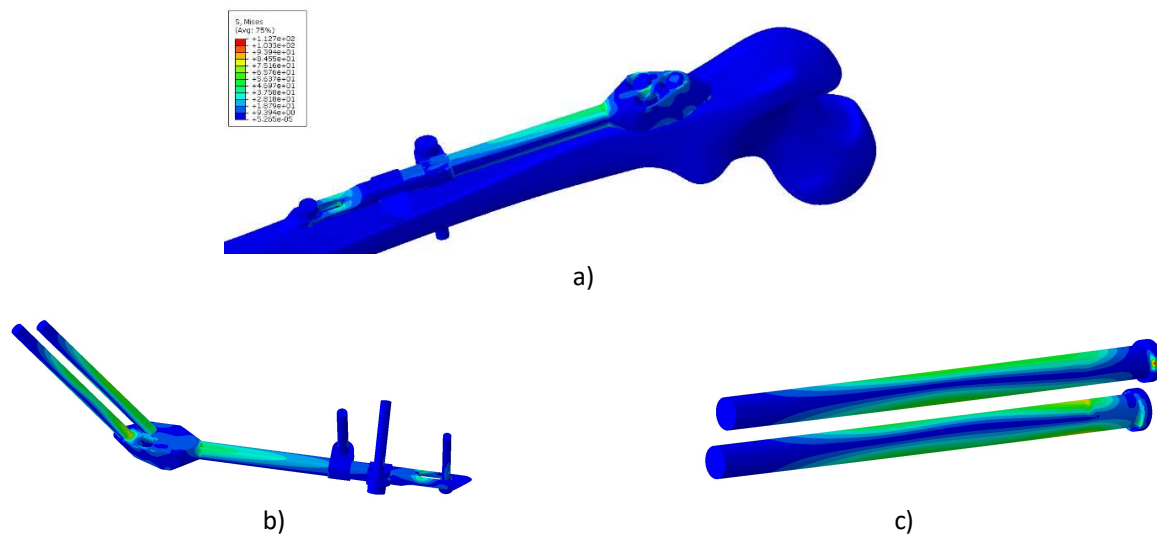


Fig. 4.17. Equivalent stress in a) femur-SIF assembly, b) SIF subassembly and c) dynamic hip screws.

4.2. Finite element analysis to estimate the behaviour of lattice structures used for manufacturing hip implants by SLM 3D printing method

Customized medical implants manufactured by SLM must have a fully dense metallic structure especially in the regions where the implants are attached to the human bones with titanium screws. There are some other zones of the implants where porous structures are required to ensure the osseointegration of the human tissue in the implant manufactured by SLM. Structures with a well-controlled porosity could be produced in different ways for example, by designing implants with different types of lattices (cell configurations), by adjusting the technological parameters (laser power, hatching distance, etc.) and the scanning strategy of the SLM process, or by adjusting the proportion of raw powder material (titanium, in this case) mixed with other biocompatible materials (PMMA, hydroxyapatite, etc.) [HUS13]. The research presented in this chapter, made at the Technical University of Cluj-Napoca (TUC-N), was focused on the finite element analysis of the strain and stress state

of several models that were especially designed to have different types of lattice structures (size and geometrical configuration of cells). On the basis of the research performed at TUC-N, a customized medical implant was produced from TiAl6V4 alloy for a German Medical Institute, using the SLM 250 HL machine from SLM Solutions GmbH Company (Luebeck, Germany).

Six models were elaborated using SolidWorks (Fig. 4.18). The models were distinguished by the lattice structures (cell configurations):

- rhombic (dimension of the unit cell: 1mm)
- hexagonal (dimension of the unit cell: 1.45 mm)
- square with rounded edges (dimensions of the unit cell: length = 0.8 mm; radius = 0.1 mm)
- rectangular (dimension of the unit cell: length = 1 mm; width = 0.6 mm)
- circular (dimension of the unit cell: diameter = 1 mm)
- pyramidal: (base size of the unit cell: 1.5 mm).

All the models shown in Fig. 4.18 had the extrusion and cell width of 0.2 mm, their structure being obtained by repeating the unit cell along the X and Y-axes. The models were then analyzed with the ABAQUS finite element program, with the aim of determining their stress and strain state. In all cases, a pressure load was applied perpendicular to the top surface of the models.

The mechanical behavior of the models was assumed to be elastic, being characterized by the following parameters: Young's modulus $E = 114$ GPa, Poisson's ratio $\nu = 0.31$, and yield stress $\sigma_c = 775$ MPa. These quantities correspond to the TiAl6V4 powder, as specified by the producer on its Internet site [WWW05].

Figure 4.19 illustrates the definition of the movement restrictions along the X, Y and Z-axes of the coordinate system. The displacement associated to all three axes were locked by selecting different faces of the model.

The pressure acting on the top surface of the model was defined according to the relationship:

$$p = F / A_p \quad (4.3)$$

in which a force $F = 3200$ N was considered (four-times higher than the gravitational load corresponding to a body weight of 80 kg).

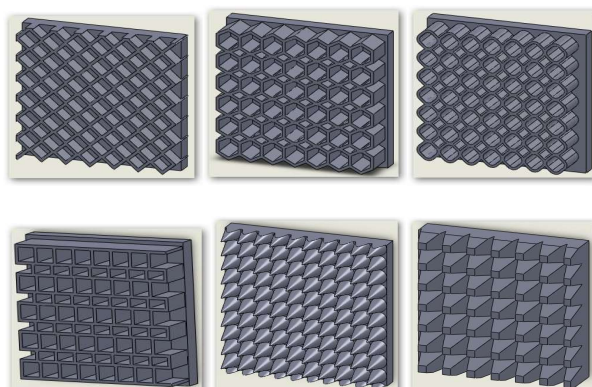


Fig. 4.18. Models with different lattice structures elaborated with

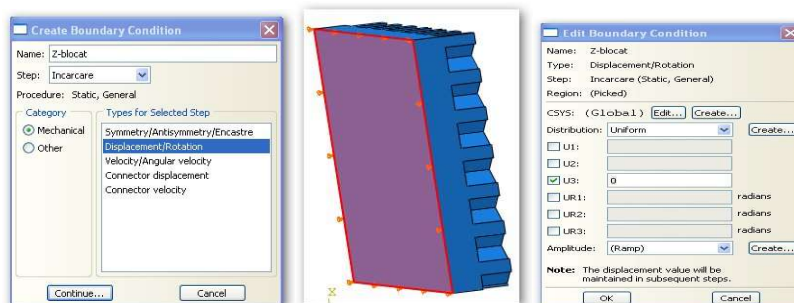


Fig. 4.19. Motion restriction applied along the Z-axis



Fig. 4.20. Pressure load applied in the analysis

As for the size of the contact area A_p [mm²], it was evaluated for each type of lattice using the measurement tools provided by SolidWorks. The pressure evaluated with Eq (4.3) was applied to each model, as shown in Figure 4.20.

This project has been funded with support from the European Commission. This publication [communication] reflects the views only of the authors, and the Commission cannot be held responsible for any use which may be made of the information contained therein.

Figure 4.21 shows the finite element mesh used in the analysis. Tetrahedral finite elements with an average dimension of 0.25 mm and a maximum curvature deviation of about 0.1 mm were generated.

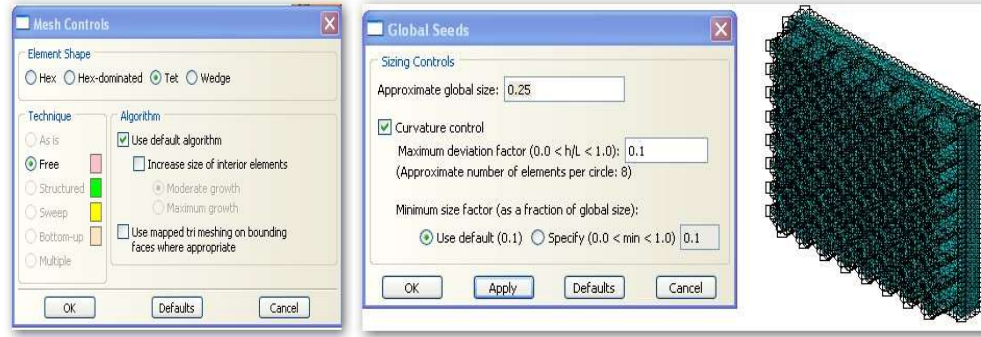


Fig. 4.21. Control of the element type and mesh size

The distribution of displacements, von Mises equivalent stress, and equivalent strain were computed for each model shown in Figure 4.18. The finite element analysis allowed recommending the optimum values in the standard limits that exist in this field. The von Mises equivalent stress results from the 5th strength theory:

$$\sigma_{ech} = \sqrt{\frac{1}{2}[(\sigma_x - \sigma_y)^2 + (\sigma_y - \sigma_z)^2 + (\sigma_z - \sigma_x)^2 + 3(\tau_{xy}^2 + \tau_{yz}^2 + \tau_{zx}^2)]} \geq 0; \sigma_{ech} \leq \sigma_c \quad (4.4)$$

The density of stress energy was also evaluated using the following relationship:

$$E_{def} = \frac{1}{2} \sigma_{ech} \times \varepsilon_{ech} \quad (4.5)$$

in which E_{def} is the density of the stress energy, σ_{ech} is the von Mises equivalent stress, and ε_{ech} is the associated equivalent strain.

According to Fig. 4.22, the values of the von Mises equivalent stress were considerably lower than the yield stress $\sigma_c = 775$ MPa of the TiAl6V4 alloy. The minimum value of the equivalent stress (102.50 MPa) was obtained in the case of the rhombic unit cell, while the maximum value (278.56 MPa) was obtained in the case of the conical unit cell. If a strength value of 212 MPa of the trabecular bone is considered, the optimum solution would be to

produce a medical implant having a rhombic unit cell [WWW06]. The values of the displacement and equivalent strain were negligible in all cases, being too low for affecting the bone and the medical implant made by SLM from TiAl6V4 powder [WWW06]. Based on the results presented above, a customized implant was manufactured by SLM from TiAl6V4 material for a German Medical Institute, using the SLM 250 HL machine from SLM Solutions GmbH Company from Luebeck (Fig. 4.23).

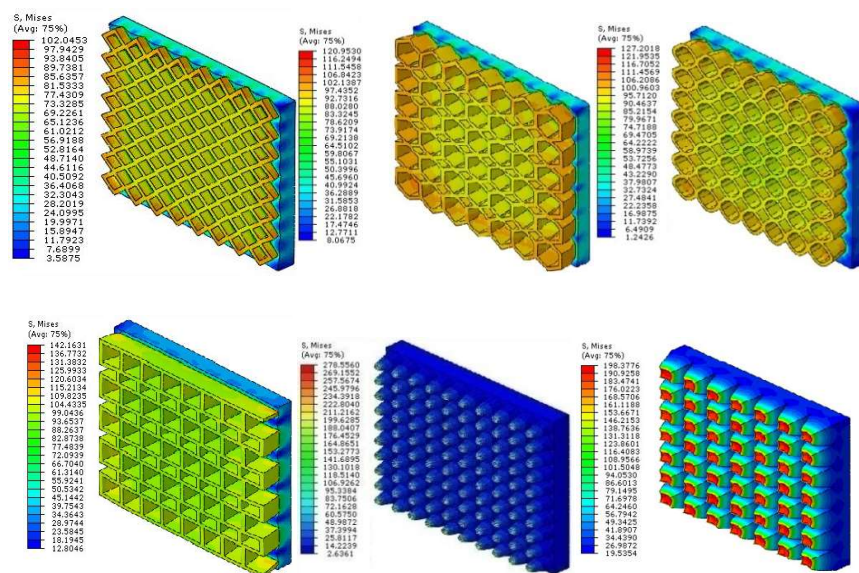


Fig. 4.22. Distribution of the von Mises equivalent stress determined by Abaqus for each type of lattice structure



Fig. 4.23. Customized implant produced from Ti6Al4V powder on the SLM 250 HL machine

This project has been funded with support from the European Commission. This publication [communication] reflects the views only of the authors, and the Commission cannot be held responsible for any use which may be made of the information contained therein.

References

- [AND10] An, Y. H., Draughn, R. A., Mechanical Testing of Bone and the Bone–Implant Interface, CRC Press, 2010.
- [BIZ18] Bi, Z., Finite Element Analysis Applications. A Systematic and Practical Approach, New York, Academic Press, 2018.
- [BUR76] Burstein, AH, Reilly, DT, Martens, M (1976). Aging of bone tissue: mechanical properties: J Bone Joint Surg Am. pp 58-82.
- [CAI20] Caia, L., Zhang, Y., Zheng, W., Wang, J., Guo, X., Fenga, Y., A novel percutaneous crossed screws fixation in treatment of Day type II crescent fracture–dislocation: A finite element analysis, Journal of Orthopaedic Translation, Vol. 20, 2020, pp. 37-46.
- [FUN93] Fung, Y. C., Biomechanics: Mechanical Properties of Living Tissues; 2nd edition, Springer Verlag, Berlin Heidelberg, 1993.
- [GIB99] Gibson L. J., Ashby M. L, Cellular solids. Structures and properties – Second edition, Cambridge University Press, 1999.
- [HEL08] B. Helgason, E. Perilli, E. Schileo, F. Taddei, S. Brynjólfsson, M. Viceconti, Mathematical relationships between bone density and mechanical properties: a literature review. Clinical Biomechanics, 23, 135-146, 2008.
- [HUS13] Hussein, A., Hao, L., Yan, C., Everson, R., Young, P., "Advanced lattice support structures for metal additive manufacturing", Journal of Materials Processing Technology, vol. 213, (2013), pp. 1019–1026.
- [ISP2016] Ispas, A., Cosma, C., Craciun, A., Constantiniuc, M., Lascu, L., Leordean, D., Vilau, C. (2016) Influence of Ti-Ceramic or Ti-Composite crown on stress distribution: finite element study and additive manufacturing, J Optoelectron Adv M; 18(9-10), pp. 904-912.
- [KOM05] Komatsubara et al (2005). Human parathyroid hormone (1–34) accelerates the fracture healing process of woven to lamellar bone replacement and new cortical shell formation in rat femora: Bone 36.4. pp 678-687.
- [KOR10] Korunović, N., Trajanović, M., Mitković, M., & Vulović, S. (2010). From CT scan to FEA model of human femur. IMK-14-Istraživanje i razvoj, 16(2), 45-48 (In Serbian)

- [KOR13] Korunovic, N., Trajanovic, M., Stevanovic, D., Vitkovic, N., Stojkovic, M., Milovanovic, J., Ilic, D. (2013). Material characterization ISSUES in FEA of long bones. SEECCM III - 3rd South-East European Conference on Computational Mechanics, Kos, Greece, 12. - 14. June 2013.
- [KOR15] Korunović, N., Trajanović, M., Mitković, M. Vitković, N., Stevanović, D. (2015). A parametric study of selfdynamisable internal fixator used in femoral fracture treatment, Proceedings of NAFEMS World Congress 2015 inc. the 2nd International SPDM Conference, San Diego, CA, 2015, paper 359, pp 1-17
- [KOR16] Korunović, N., Stojković, M., Milovanović, J., Vitković, N., Trifunović, M., Manić, M., & Trajanović, M. (2016). Bioengineering and tire design related research at LIPS laboratory: A summary of results. Journal of Serbian Society for Computational Mechanics, 10(1), 71-101.
- [KOR19a] Korunovic, N., Marinkovic, D., Trajanovic, M., Zehn, M., Mitkovic, M., & Affatato, S. (2019). In Silico Optimization of Femoral Fixator Position and Configuration by Parametric CAD Model. Materials, 12(14), 2326. M22, <https://doi.org/10.3390/ma12142326>
- [KOR19b] Korunovic, N., Trajanovic, M. & Mitkovic, M. (2019). A Parametric Study of Selfdynamisable Internal Fixator Used in Femoral Fracture Treatment, NAFEMS Benchmark, October 2019, pp. 38-44., <https://www.nafems.org/publications/benchmark/archive/october-2019/>
- [KOR53] Ko, R (1953). The tension test upon the compact substance of the long bones of human extremities: J Kyoto Pref Med Univ. 53. pp 503–525.
- [MIC10] Micic, I.; Mitkovic, M.; Park, I.H.; Mladenovic, D.; Stojiljkovic, P.; Golubovic, Z.; Jeon, I.H. Treatment of subtrochanteric femoral fractures using Selfdynamisable internal fixator. Clin. Orthop. Surg. 2010, 2, 227–231.
- [MIL09] Milovanović, J., Trajanović, M., Vitković, N., & Stojković, M. (2009). Rapid prototyping tehnologije i materijali za izradu implantata. IMK-14 - Istraživanje i razvoj, 15(1-2), 23-30.
- [MIL15] Milovanović, J., Stojković, M., & Trajanović, M. (2015). Applicability analysis of additive manufacturing processes in the fabrication of anatomically shaped lattice scaffolds. Facta Universitatis, Series: Mechanical Engineering, 13(3), 295-305.
- [MIL20] Milovanović, J., Stojković, M., Trifunović, M., & Vitković, N. (2020). REVIEW OF BONE SCAFFOLD DESIGN CONCEPTS AND DESIGN METHODS. Facta Universitatis, Series: Mechanical Engineering.

- [MIR17] Miron-Borzan, C.S., Sabau, E., Mera, M., Berce, P. (2017) Research Regarding the Manufacturing through AM Technologies of an Implant for Cervical Disc Replacement. MATEC Web of Conferences; 137:02008.
- [MIS02] Mischler, S, Pax, G (2002). Tribological behavior of titanium sliding against bone: European Cells and Materials 3.1. pp. 28-29.
- [MIT12] Mitkovic, M.; Milenkovic, S.; Micic, I.; Mladenovic, D.; Mitkovic, M. Results of the femur fractures treated with the new selfdynamisable internal fixator (SIF). Eur. J. Trauma Emerg. Surg. 2012, 38, 191–200.
- [MOR03] E.F. Morgan, H.H. Bayraktar, T.M. Keaveny, Trabecular bone modulus-density relationships depend on anatomic site. Journal of Biomechanics, 36, 897-904, 2003.
- [OLD12] Oldani, Carlos, Dominguez, Alejandro (2012). Titanium as a Biomaterial for Implants: Recent Advances in Arthroplasty, Dr. Samo Fokter (Ed.), InTech. pp 149-162.
- [PAR19] Park, D.W., Lim, A., Park, J.W., Lim, K.M., Kang, H.G., Biomechanical Evaluation of a New Fixation Type in 3D-Printed Periacetabular Implants using a Finite Element Simulation, Applied Sciences, Vol. 9, No. 5, 2019, p. 820.
- [PET18] Petrović S., Korunović N. (2018) Imaging in Clinical and Preclinical Practice. In: Zivic F., Affatato S., Trajanovic M., Schnabelrauch M., Grujovic N., Choy K. (eds) Biomaterials in Clinical Practice. Springer, pp 539-572, Cham
- [SCH08] E. Schileo, E. Dall'Ara, F. Taddei, A. Malandrino, T. Schotkamp, M. Baleani, M. Viceconti, An accurate estimation of bone density improves the accuracy of subject-specific finite element models. Journal of Biomechanics, 41, 2483-2491, 2008.
- [STO09] Stojkovic M., Trajanovic M., Vitkovic N., Milovanovic J., Arsic S, Mitkovic M., Referential geometrical entities for reverse modeling of geometry of femur, Proceedings of VIPIMAGE2009, Porto, Portugal, Oct 2009, p.p. 189-194
- [STO13] Stojkovic, M., Korunovic, N., Trajanovic, M., Milovanovic, J., Trifunovic, M., Vitkovic, N. (2013). Design Study Of Anatomically Shaped Latticed Scaffolds For The Bone Tissue Recovery. SEECCM III - 3rd South-East European Conference on Computational Mechanics, Kos, Greece, 12. - 14. June 2013.
- [THO17] Thompson, M.K., Thompson, F.M., ANSYS Mechanical APDL for Finite Element Analysis, New York, Butterworth-Heinemann, 2017.
- [VIN85] Vincentelli, R, Grigorov, M (1985). The effect of Haversian remodeling on the tensile properties of human cortical bone: J Biomech. 18: pp 201–207

- [VIT13] Vitković, N., Milovanović, J., Korunović, N., Trajanović, M., Stojković, M., Mišić, D., Arsić, S. (2013). Software system for creation of human femur customized polygonal models. *Computer Science and Information Systems*, 10(3), 1473-1497.
- [VUL11] Vulovic, S., Korunovic, N., Trajanovic, M., Grujovic, N., & Vitkovic, N. (2011). Finite element analysis of CT based femur model using finite element program PAK. *Journal of the Serbian Society for Computational Mechanics*, 5(2), 160-166.
- [WWW01] <https://3dprint.com/43103/3d-printed-cast>
- [WWW02] <http://2015.igem.org/wiki/images/2/24/CamJIC-Specs-Strength.pdf>
- [WWW03] https://en.spectrumfilaments.com/data/include/cms/Premium_PLA_TDS_EN.pdf
- [WWW04] <https://www.materialise.com/en/medical/mimics-innovation-suite>
- [WWW05] https://www.slm-solutions.com/fileadmin/Content/Powder/MDS/MDS_Ti-Alloy_Ti6Al4V__ELI_0719_EN.pdf
- [WWW06] https://ota.org/sites/files/2018-06/G08_Biomechanics-%20Edited%20with%20Questions%20%5BCompatibility%20Mode%5D.pdf
- [WWW07] https://webbuilder5.asiannet.com/ftp/2684/sheet_07-08_en_provisional.pdf